Brain-resident memory T cells represent an autonomous cytotoxic barrier to viral infection

Karin Steinbach,[1]* Ilena Vincenti,[1]* Mario Kreutzfeldt,[1] Nicolas Page,[1] Andreas Muschaweckh,[2] Ingrid Wagner,[1] Ingo Drexler,[3] Daniel Pinschewer,[4] Thomas Korn,[2,5] and Doron Merkler[1,6]

[1]Departement de Pathologie et Immunologie, Centre Medical Universitaire, University of Geneva, 1211 Geneva, Switzerland
[2]Klinikum rechts der Isar, Department of Experimental Neuroimmunology, Technical University of Munich, 81675 Munich, Germany
[3]Institute of Virology, University Hospital Düsseldorf, Heinrich-Heine-University, 40225 Düsseldorf, Germany
[4]Department of Biomedicine, University of Basel, 4056 Basel, Switzerland
[5]Munich Cluster of Systems Neurology (SyNergy), 81377 Munich, Germany
[6]Division of Clinical Pathology, Geneva University Hospital, 1211 Geneva, Switzerland

Tissue-resident memory T cells (T_{RM}) persist at sites of prior infection and have been shown to enhance pathogen clearance by recruiting circulating immune cells and providing bystander activation. Here, we characterize the functioning of brain-resident memory T cells (bT_{RM}) in an animal model of viral infection. bT_{RM} were subject to spontaneous homeostatic proliferation and were largely refractory to systemic immune cell depletion. After viral reinfection in mice, bT_{RM} rapidly acquired cytotoxic effector function and prevented fatal brain infection, even in the absence of circulating $CD8^+$ memory T cells. Presentation of cognate antigen on MHC-I was essential for bT_{RM}-mediated protective immunity, which involved perforin- and IFN-γ–dependent effector mechanisms. These findings identify bT_{RM} as an organ-autonomous defense system serving as a paradigm for T_{RM} functioning as a self-sufficient first line of adaptive immunity.

Immunological memory is characterized by a more rapid and efficient response to previously encountered pathogens. Thereby, memory recall responses protect against infections that can otherwise cause disease or even death in immunologically naive hosts. Memory $CD8^+$ T cells (T_M) are instrumental for the rapid detection and eradication of intracellular pathogens. Several subsets of T_M have been identified based on their migration patterns, anatomical location, and functional specialization (Mueller et al., 2013). Historically, memory T cells have been divided into central memory T cells (T_{CM}) and effector memory T cells (T_{EM}; Sallusto et al., 1999). T_{CM} home to secondary lymphoid organs, exhibit high proliferative capacity upon reencountering cognate antigen, and serve as a self-replenishing pool that gives rise to other memory T cell subsets (Graef et al., 2014). Conversely, T_{EM} do not express the homing receptors characteristic of T_{CM}, recirculate through the body, and can provide immediate effector function (Sallusto et al., 1999). Recently, tissue-resident memory T cells (T_{RM}) have been identified as an additional subset of memory T cells that does not recirculate, but persists at sites of previous infection, such as skin and mucosal tissues (Schenkel and Masopust, 2014b; Park and Kupper, 2015), as well as the brain (Wakim et al., 2010). T_{RM} from various organs, including the brain show overlapping transcriptional profiles with a core transcriptional signature (Schenkel and Masopust, 2014a), distinguishing them from circulating T_M (Wakim et al., 2012; Mackay et al., 2013). In most nonlymphoid tissues, T_{RM} outnumber patrolling T_{EM} and constitute the largest component of T cell memory (Steinert et al., 2015). Their persistence in organs is mediated by specific adhesion molecules, such as CD103 (Integrin αE; Gebhardt et al., 2009; Casey et al., 2012; Mackay et al., 2013) and loss of tissue egress receptors from the cell surface (Skon et al., 2013; Mackay et al., 2015a). Bona fide T_{RM} have been described to express CD69, which antagonizes the tissue egress receptor sphingosine 1-phosphate receptor 1 (S1P1; Mackay et al., 2015a). Surface expression of CD103 seems specific for T_{RM}, but not all T_{RM} express the molecule. Long-lived $CD103^-$ T_{RM} have been described in secondary lymphoid organs (Schenkel et al., 2014b), in the gut (Bergsbaken and Bevan, 2015), and in the female reproductive tract (Steinert et al., 2015). CD103 expression has been associated with tissue retention (Wakim et al., 2010; Casey et al., 2012; Mackay et al., 2013), epithelial localization (Gebhardt et al., 2009; Sheridan et al., 2014) and function (Wakim et al., 2010; Laidlaw et al., 2014; Bergsbaken and Bevan, 2015), but it remains elusive whether CD103 expression is causally linked to these characteristics. The generation and maintenance of T_{RM} is dependent on IL-7 and IL-15-mediated signals (Mackay et al., 2013; Adachi et al., 2015), however, whether T_{RM} undergo

*K. Steinbach and I. Vincenti contributed equally to this paper.

Correspondence to Doron Merkler: doron.merkler@unige.ch

Abbreviations used: bT_{RM}, brain-resident T_{RM}; GKO, IFN-γ knockout; LCMV, lymphocytic choriomeningitis virus; MVA, modified vaccinia virus Ankara; PKO, perforin-knockout; S1P1, sphingosine 1-phosphate receptor 1; T_{RM}, tissue-resident memory T cells.

The Rockefeller University Press $30.00
J. Exp. Med. 2016 Vol. 213 No. 8 1571–1587
www.jem.org/cgi/doi/10.1084/jem.20151916

Supplemental material can be found at:
http://doi.org/10.1084/jem.20151916

homeostatic proliferation to maintain a stable population has so far not been demonstrated.

T_{RM} accelerate and improve pathogen clearance upon reinfection (Gebhardt et al., 2009; Jiang et al., 2012; Shin and Iwasaki, 2012; Wakim et al., 2012; Sheridan et al., 2014), but the underlying mechanisms remain a subject of ongoing investigation. Reactivation of T_{RM} by cognate antigen leads to the production of inflammatory cytokines, such as IFN-γ. Consequently, antiviral genes are induced and additional immune cells are rapidly recruited from the circulation (Schenkel et al., 2013, 2014a; Ariotti et al., 2014). The currently prevailing concept therefore suggests that T_{RM} represent a tissue-restricted surveillance system with the capacity to alert circulating T_M in case of reinfection (Carbone, 2015). Conversely, a potential function of T_{RM} as directly cytotoxic antiviral effectors, and thus as an autonomous immunological barrier to viral reinfection, has so far been mostly dismissed, owing to the small number of T_{RM}, which persist after primary infection, although reports suggest a direct antiviral function of skin T_{RM} (Liu et al., 2010; Jiang et al., 2012; Mackay et al., 2015b).

Here, we studied brain T_{RM} (bT_{RM}) in established mouse models of viral CNS infection. Antiviral bT_{RM} persisted in the CNS for prolonged periods of time, underwent homeostatic proliferation, and served as a potent cellular barrier of antigen-specific immunity, which achieved virus control independently of circulating T cells. Rapid bT_{RM}-mediated virus clearance relied on IFN-γ expression and perforin-mediated cytotoxicity and protected mice from immunopathological CNS disease. Our findings suggest that bT_{RM} can act as an organ-autonomous defense system of the CNS.

RESULTS

$CD103^+$ and $CD103^-$ bT_{RM} persist after cerebral viral infection and accelerate pathogen clearance during infection with a related virus

To study the generation and function of bT_{RM}, we infected mice intracerebrally (i.c.) with a genetically engineered, attenuated lymphocytic choriomeningitis virus (LCMV) variant (rLCMV; Pinschewer et al., 2003). As previously shown (Pinschewer et al., 2010), i.c. administered rLCMV rapidly drained to the periphery and triggered a potent peripheral antiviral $CD8^+$ T cell response, which resolved the brain infection within ten days (Fig. 1 A). Thereafter, T cell numbers in the brain contracted, but a population of T_M persisted in stable number and frequency from 6 wk after infection onwards (Fig. 1, B and C). At that time point, most persisting T_M cells expressed CD69, a prototypic T_{RM} marker. $CD69^+$ brain T_M expressed high Bcl-2 levels, and many were Granzyme B–positive (59 ± 3%), whereas most of them were specific for the immunodominant LCMV epitope $NP_{396-404}$ (82 ± 5%). However, only about half of these cells (50 ± 10%) expressed CD103 (Fig. 1 D and Fig. S1). Both $CD103^+$ and $CD103^-$ $CD69^+$ T_M subsets persisted in stable relative proportions over time (Fig. 1 E). Analogously to the endogenous $CD8^+$ T cell pool, both $CD103^+$ and $CD103^-$ brain T_M subsets were found in adoptively transferred $CD8^+$ TCR transgenic P14 or OT-1 cells, respectively, after i.c. infection with rLCMV variants encoding the respective cells' cognate epitopes (Fig. 1 F). Furthermore, $CD103^+$ and $CD103^-$ OT-1 brain T_M were generated after intrathecal infection with a modified vaccinia virus (MVA; Rothhammer et al., 2014) expressing OVA (Fig. 1 G). CD69 expression correlated with exclusion from staining with i.v. administered fluorescent antibody (Anderson et al., 2014; Fig. 1 H) and extravascular $CD8^+$ T cells identified by immunostaining on brain sections expressed CD69 (95 ± 3%; $n = 3$ mice). Furthermore, most brain $CD69^+$ T_M cells were refractory to depletion by peripherally administered depleting anti-CD8 antibody (Fig. 1 I). Altogether, this demonstrated that the vast majority of $CD69^+$ T_M cells in brain were bona fide T_{RM} (from now on referred to as bT_{RM}).

To investigate the protective role of bT_{RM} upon brain reinfection, we generated rLCMV memory mice by either i.v. or co-infection (i.c. + i.v.; Fig. 2 A). Co-infection was used to assure similar generation of circulating T_M. Indeed, both infection routes led to similar frequencies of D^b-$NP_{396-404}$ LCMV-specific T_M in peripheral blood (Fig. 2 B). However, in contrast to bT_{RM} generated upon i.c. infection, only limited numbers of T_M cells were present in the brain after i.v. infection with rLCMV (Fig. 2, C and D). These latter cells were susceptible to depletion by peripherally administered anti-CD8a antibody (unpublished data) demonstrating that T_M detectable in the brain after i.v. rLCMV infection are in equilibrium with the circulation and do not represent bona fide bT_{RM}. In addition, brain circulating T_M generated by i.v. infection failed to up-regulate CD103 and contained a lower percentage of D^b-$NP_{396-404}$–specific cells than bT_{RM} generated by i.c. infection (Fig. 2 E). Next, rLCMV memory mice with bT_{RM} (i.c. + i.v. rLCMV co-infection) or without bT_{RM} (i.v. rLCMV infection) were i.c. challenged with pathogenic WT LCMV (LCMVwt), which shared the immunodominant $NP_{396-404}$ epitope with rLCMV (Fig. 2 F). When analyzed 3 d later, rLCMV memory mice with bT_{RM} exhibited significantly lower LCMV virus load in the brain than rLCMV memory mice with only circulating T_M. This indicated that the generation of bT_{RM} provided an advantage during reinfection.

$CD103^+$ and $CD103^-$ bT_{RM} persist in proximity to anatomical barriers and undergo homeostatic proliferation

We next analyzed the spatial distribution of bT_{RM} on brain sections by immunohistochemistry. bT_{RM} were preferentially detected at brain surface structures, such as meninges and choroid plexus, around the ventricles or at anatomical borders between different brain regions (Fig. 3 A). Only a small fraction of bT_{RM} was in direct contact with vascular endothelium (14 ± 3%; Fig. 3 A), but most bT_{RM} localized in close proximity to vessels and brain surface structures, or both (Fig. 3 B). Quantification of $CD103^+$ and $CD103^-$ bT_{RM} in the analyzed areas did not reveal a correlation of CD103 expression with

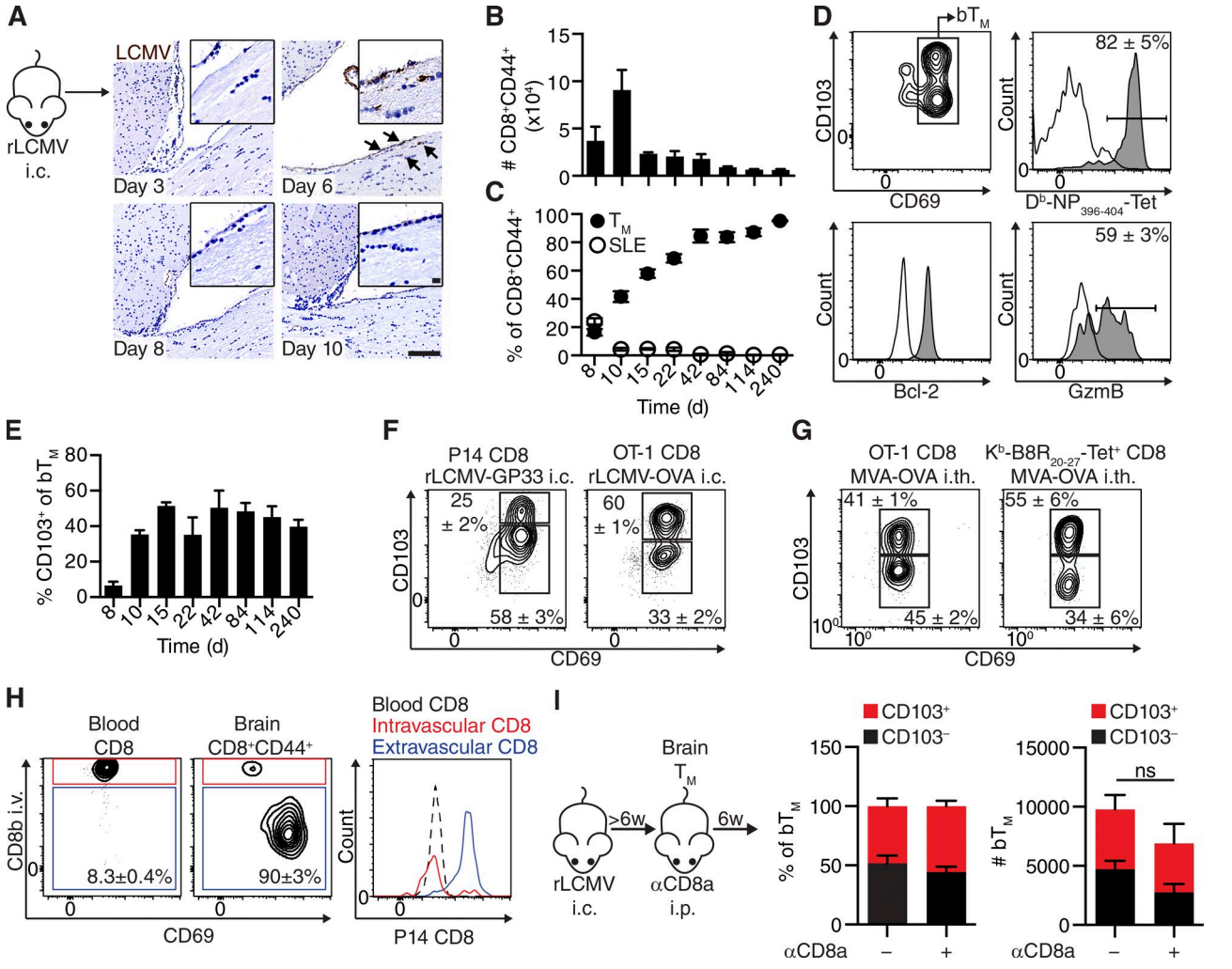

Figure 1. **CD103$^+$ and CD103$^-$ T_M persist in the brain after cerebral viral infection.** (A) Representative brain sections of WT mice immunostained for LCMV nucleoprotein (arrows) at indicated days after rLCMV i.c. infection. Bars: 100 µm; (inset) 20 µm. (B–F) Flow cytometric analysis of brain-derived CD8$^+$ T cells after rLCMV i.c. infection (as in Fig. S1). (B) Quantification of brain CD8$^+$ T cell numbers and (C) frequencies of T_M and short-lived effectors (SLE) at indicated days (d) after infection. (D) CD69$^+$ brain T_M (bT_M) were analyzed for surface expression of CD103, binding of D^b-$NP_{396-404}$-tetramer, and intracellular expression of Bcl-2 and Granzyme B (GzmB; filled histograms, antibody stainings; open histograms, staining controls) 6 wk after infection. Numbers indicate frequencies of positive cells (mean ± SEM; n = 3 mice). (E) Frequencies of CD103$^+$ bT_M at indicated days (d) after infection. (F and G) P14 or OT-1 TCR transgenic CD8$^+$ T cells were adoptively transferred into naive WT mice 24 h before infection with indicated viruses. CD69 and CD103 surface expression on the adoptively transferred T cells (CD45.1$^+$) and on endogenous MVA-specific CD8$^+$ T cells (Kb-$B8R_{20-27}$-Tet$^+$) in brains was analyzed by flow cytometry at 14 (F) or 6 wk (G) after infection. The frequencies of cells in the different gates are indicated (mean ± SEM; n = 4–5 mice per group). (H) 3 mo after infection with rLCMV i.c., anti-CD8b-PE was injected i.v. and PE-labeled CD8b$^+$ T cells were measured in the blood and the brain by flow cytometry. Representative plots of CD8b-positive (intravascular, red) and -negative (extravascular, blue) CD8a$^+$ T cells in relation to CD69 expression are shown. The frequencies of cells in the different gates are indicated (mean ± SEM; n = 4–5 mice per group). (I) rLCMV i.c. infected WT mice were treated with anti-CD8a depleting antibody i.p. 6 wk after infection. Frequencies and numbers of CD103$^+$ and CD103$^-$ brain T_M (CD8$^+$CD44$^+$CD69$^+$) were analyzed by flow cytometry 6 wk later. (B, E, and I) Bars represent mean + SEM (n = 5–6 mice per group). One representative of (A, D, H, and I) or data pooled from (B, C, and E) at least two independent experiments is shown. (F and G) Experiments were performed once. For flow cytometric gating strategy see Fig. S1.

their localization (Fig. 3 C). Interestingly, a consistent fraction of bT_{RM} expressed proliferation marker Ki-67 (9 ± 1%) long after virus clearance (Fig. 3 D). bT_{RM} at brain surface structures expressed Ki-67 more frequently than bT_{RM} localized in brain parenchyma (Fig. 3 E). Previous studies have shown that IL-7– and IL-15–dependent longevity and homeostatic proliferation are maintaining central memory T cells by Stat5 signaling (Burchill et al., 2003; Willinger et al., 2005; Hand et al., 2010). Indeed, a fraction of brain T cells showed Stat5 phosphorylation (26 ± 7%). Similarly to Ki-67$^+$ T cells, we observed an increased proportion of P-Stat5$^+$ T cells at brain surface structures (Fig. 3 F). Using histocytometry (Fig. S2),

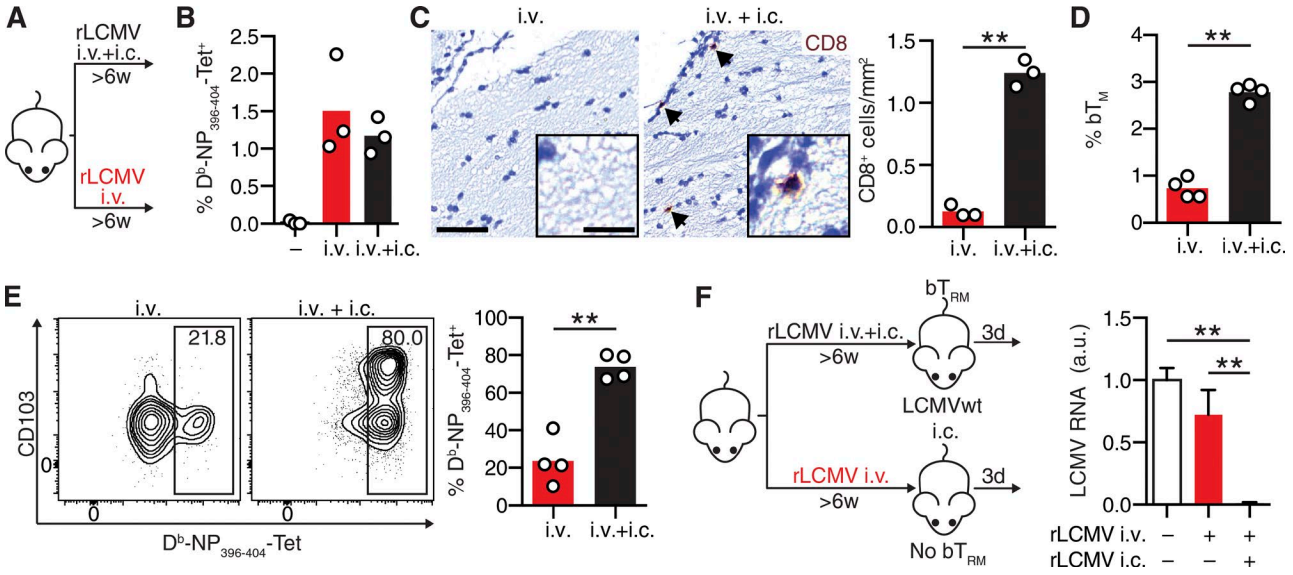

Figure 2. **Brain T_{RM} generated by local infection are associated with accelerated virus clearance.** (A) WT mice were infected with rLCMV i.v. or co-infected i.v. + i.c., and brains were analyzed at least 6 wk later. (B) Frequencies of D^b-NP396-404–specific $CD8^+$ T cells in peripheral blood. (C) Representative images of immunostained brain sections for $CD8^+$ T cells (arrows) and quantification thereof. Bars: 100 µm; (inset) 20 µm. (D) Frequencies of bT_{RM} ($CD8^+CD44^+CD69^+$) in total brain leukocytes as determined by flow cytometry (as in Fig. S1). (E) Representative flow cytometry plot of CD103 and D^b-NP396-404-tetramer on brain T_M (left) and frequencies of D^b-NP396-404–specific brain $CD8^+$ T cells ($CD8^+CD44^+CD69^+$; right). Numbers represent frequencies (%) of positive events. (F) WT mice were infected with rLCMV as in A and challenged with LCMVwt i.c. 6 wk later. Naive WT mice infected with LCMVwt i.c. were used as controls. Quantification of LCMV RNA by qPCR in the brain (normalized to the virus load in naive mice infected with LCMVwt i.c. = 1). (B–E) Bars represents mean and each symbol represents an individual mouse (n = 3–4 mice per group) or (F) bars represent mean + SEM. (n = 5 mice per group). **, $P < 0.01$, one-way ANOVA followed by Tukey's multiple comparisons test. One out of at least two independent experiments is shown.

we could confirm that meninges contained a higher frequency of P-Stat5$^+$ T cells than internal brain structures (Fig. 3 G). Altogether, this indicates that Stat5-driven homeostatic proliferation contributes to the maintenance of the long-lived bT_{RM} population preferentially at brain surface structures.

bT_{RM} autonomously clear pathogenic LCMV challenge independently of circulating T_M cells

To assess the contribution of circulating $CD8^+$ T cells to virus control in the brain, we treated a group of rLCMV memory mice with anti-CD8 depleting antibody before LCMVwt i.c. challenge (Fig. 4 A). rLCMV memory mice with bT_{RM} and circulating T_M contained significantly more T cells in the brain after challenge than mice with only circulating T_M (Fig. 4, B and C). As expected (Schenkel et al., 2013), the numbers of brain-infiltrating T cells in the former group were significantly reduced when circulating T_M were depleted. This indicated that about half of the brain $CD8^+$ T cells after LCMVwt challenge of nondepleted mice originated from a recruitment of circulating T_M, whereas the other half represented bT_{RM} and their progeny. Furthermore, 47 ± 13% of bT_{RM} expressed proliferation marker Ki-67 after LCMVwt i.c. challenge (Fig. 4 D), indicating that a substantial fraction of bT_{RM} entered the cell cycle upon antigen reencounter in the CNS. During LCMV i.c. challenge, both $CD103^+$ and $CD103^-$ bT_{RM} expanded in similar proportions and showed equal potential for Ki-67 up-regulation (Fig. 4, E and F). Intriguingly, rLCMV memory mice with bT_{RM} but lacking circulating T_M, cleared virus from the brain equally efficiently as mice with both bT_{RM} and circulating T_M (Fig. 4, C, G, and H). This suggested that recruitment of circulating T_M was not required for bT_{RM}-mediated virus clearance from the brain. Conflicting reports exist about T_{RM} dependency on $CD4^+$ T help in different organs (Jiang et al., 2012; Laidlaw et al., 2014). To address the role of $CD4^+$ T cells for the generation and function of bT_{RM}, we depleted $CD4^+$ T cells either during primary i.c. infection with rLCMV or performed a combined depletion of circulating $CD4^+$ and $CD8^+$ T cells during LCMVwt i.c. challenge. bT_{RM} numbers, as well as bT_{RM}-mediated rapid virus clearance during LCMVwt i.c. challenge, was not affected in the absence of $CD4^+$ T cell help during bT_{RM} generation or challenge with LCMVwt (Fig. 5, A–L). Furthermore, to exclude that recruited NK cells contribute to virus clearance, we depleted NK cells in addition to circulating T cells during LCMVwt i.c. challenge. However, virus clearance was unimpaired in animals containing bT_{RM} but not circulating T and NK cells (Fig. 6, A–E), demonstrating that LCMVwt control relied on bT_{RM}.

bT_{RM}–mediated virus clearance is dependent on presentation of cognate antigen

Next, we aimed to investigate if presentation of cognate antigen is necessary or if bystander activation and expres-

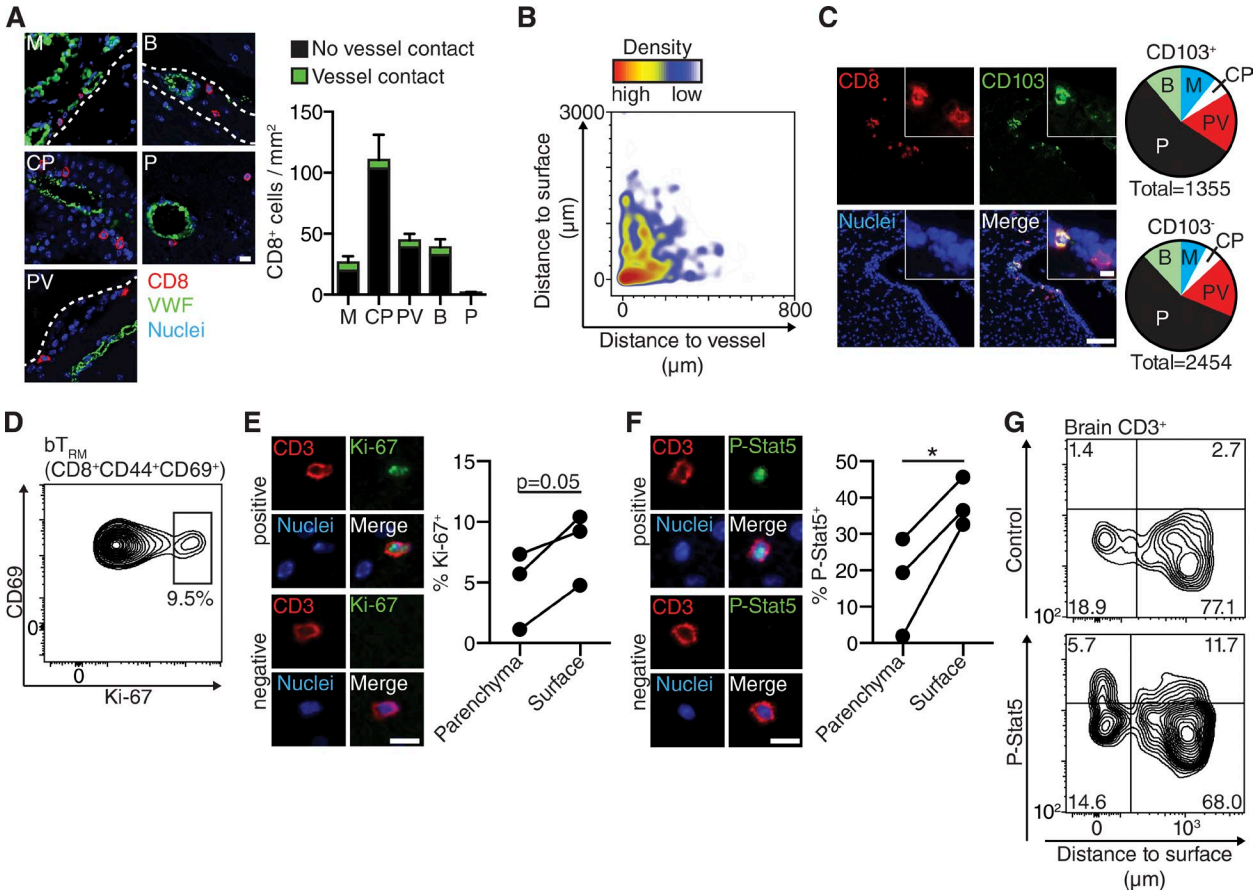

Figure 3. **bT_{RM} are localized in proximity to surface-associated structures and show homeostatic proliferation.** (A–G) Mice were infected with rLCMV i.c. to generate bT_{RM} and analyzed at least 6 wk later. (A) Regional distribution of $CD8^+$ T cells within the brain. Representative immunofluorescent images of $CD8^+$ cells localized at meninges (M), choroid plexus (CP), periventricular area (PV), interareal borders (B), and parenchyma (P), and quantification of $CD8^+$ cell density in these areas are shown. Vessels are visualized by immunostaining for Von-Willebrand Factor (VWF). Dotted lines mark the separation to the brain parenchyma. (B) Density plot of brain $CD8^+$ cells in relation to surface structures and vessels. Data are pooled from three mice. (C) Representative images of brain immunofluorescence co-staining for CD8 and CD103 and quantification of $CD103^+$ and $CD103^-$ $CD8^+$ T cells grouped in brain areas as defined in A are shown. Data are pooled from three mice (n = total counted cells). (D) Representative flow cytometry plot of Ki-67–expressing bT_{RM} ($CD8^+CD44^+CD69^+$; *n* = 4–5 mice per group). (E and F) Representative images of Ki-67– (E) or P-Stat5–positive and negative (F) T cells (left) and proportion of positive T cells at brain surface structures (meninges, choroid plexus, periventricular areas, interareal borders) in comparison to brain parenchyma (right). *, $P < 0.05$, paired two-tailed Student's *t* test. (G) Histocytometry analysis of P-Stat5–positive T cells in relation to their distance to surface (meninges). Data are pooled from three mice. Numbers represent frequencies (%) of cells in corresponding gates. Bars: (A, E, F, and inset in C) 10 µm; (C) 100 µm. For histocytometry data processing and gating strategy, see Fig. S2.

sion of antiviral genes in surrounding tissue is sufficient for bT_{RM}-mediated viral clearance. Therefore, we challenged rLCMV memory mice with a genetically engineered LCMV variant (LCMV-NP_{N400S}), in which the MHC-I anchor residue of the immunodominant epitope $NP_{396-404}$ was mutated to abrogate MHC binding (Johnson et al., 2015; Fig. 7 A), thus preventing MHC-I–restricted recognition of this virus by the vast majority of bT_{RM} (Fig. 1 D and Fig. 2 E). Accordingly, bT_{RM} expansion was reduced when LCMV-NP_{N400S} was used for challenge instead of LCMVwt (Fig. 7, B and C). In further contrast to LCMVwt i.c. challenge, bT_{RM} failed to clear the brain from LCMV-NP_{N400S} within 3 d. This was evident in increased numbers of infected cells (Fig. 7, B and D) and heightened LCMV RNA loads (Fig. 7 E). Interestingly, antiviral interferon-induced transmembrane protein 3 (Ifitm3), a marker of T_{RM}-induced antiviral state (Ariotti et al., 2014), was similarly induced after infection with LCMVwt or LCMV-NP_{N400S}, respectively (Fig. 7 F). Furthermore, infection with either of the two viruses induced up-regulation of Granzyme B (Fig. 7, G–H), as well as Ki-67 expression (Fig. 7, G and I) in bT_{RM}. This indicated that the capacity of bT_{RM} to autonomously clear brain virus infection depended on epitope-specific target recognition. Conversely, the virtually uniform activation of bT_{RM} after viral challenge occurred in a largely antigen nonspecific fashion, as D^b-NP396-404-tetramer$^+$ bT_{RM}

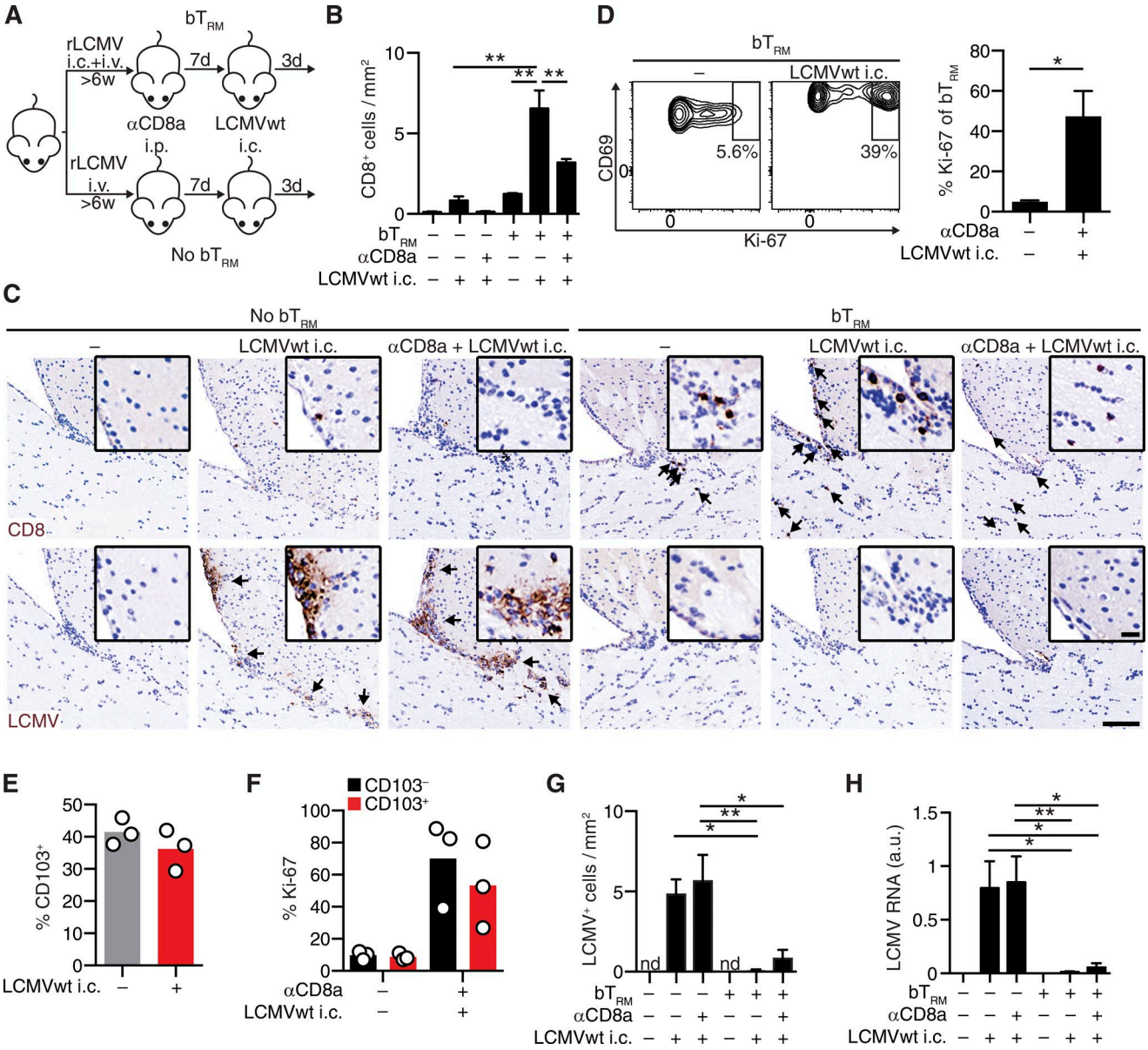

Figure 4. **bT_{RM} mediate rapid LCMV clearance independently of circulating T_M cell recruitment.** (A) WT mice were infected with rLCMV i.v. (no bT_{RM}) or i.v. + i.c. (bT_{RM}). At least 6 wk later, mice were treated i.p. with anti-CD8a depleting antibody before LCMVwt i.c. challenge or left unchallenged, and brains were analyzed 3 d later. (B) $CD8^+$ T cells quantification on immunostained brain sections in relation to the presence of bT_{RM} (+), circulating CD8 depletion (+) and LCMVwt i.c. challenge (+). (C) Representative images of CD8 (top, arrows) or LCMV (bottom, arrows) on immunostained brain sections. Bars: 100 µm; (inset) 20 µm. (D) Representative flow cytometry plot (left) and frequencies (right) of Ki-67–expressing bT_{RM} ($CD8^+CD44^+CD69^+$) after LCMVwt i.c. challenge (+) or in unchallenged control mice (–). Numbers represent frequencies of positive cells. (E) Frequencies of CD103-expressing bT_{RM} in LCMVwt i.c. challenged (+) or unchallenged (–) mice as in D. (F) Frequencies of Ki-67–expressing $CD103^+$ and $CD103^-$ bT_{RM} as in D. (D–F) Each symbol represents an individual mouse and bars indicate mean. (G) Quantification of $LCMV^+$ cells by immunohistochemistry on brain sections and (H) LCMV RNA by qPCR (normalized to naive mice infected with LCMVwt i.c. = 1) in the brain of mice as in B. Data represent mean + SEM (n = 3–5 mice for unchallenged controls (–); n = 5–6 for mice challenged with LCMVwt i.c.) *, $P < 0.05$; **, $P < 0.01$, one-way ANOVA followed by Sidak's multiple comparisons test (B, G, and H); unpaired two-tailed Student's t test (D). One representative out of at least two independent experiments is shown (B–H).

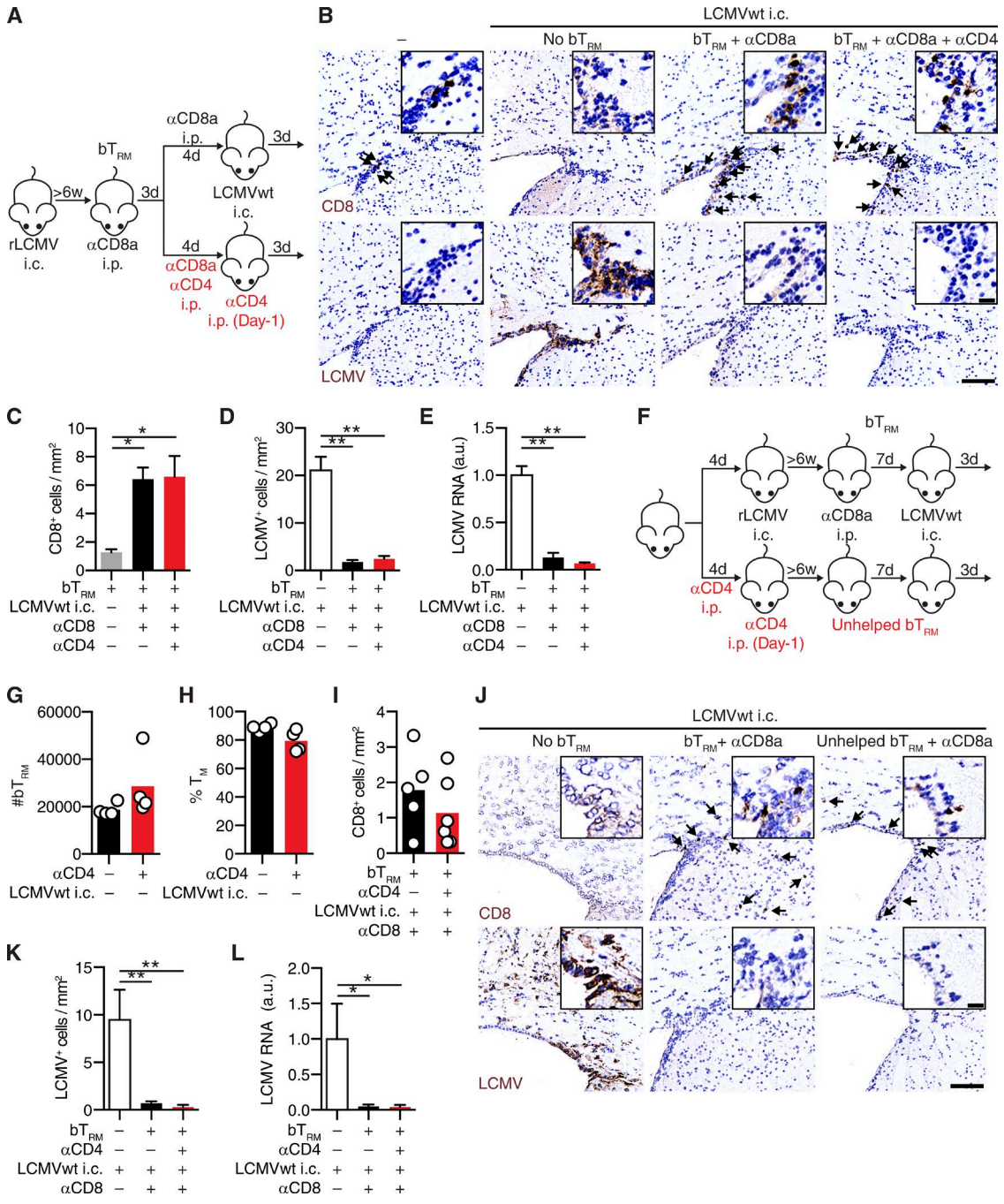

Figure 5. **bT_{RM} generation and functionality in the absence of $CD4^+$ T cell help.** (A) WT mice were infected with rLCMV i.c. 11 wk later, mice were treated with anti-CD8a alone or in combination with anti-CD4 depleting antibody i.p., and subsequently challenged with LCMVwt i.c. Naive WT mice infected with LCMVwt i.c. were used as controls. Brains were analyzed 3 d later. (B) Representative images of brain sections immunostained for CD8 (top, arrows) or LCMV (bottom). Quantification of $CD8^+$ T cells (C), $LCMV^+$ cells by immunohistochemistry (D), or LCMV RNA by qPCR (E; normalized to naive mice infected with LCMVwt i.c. = 1). (F) WT mice were treated with anti-CD4 depleting antibody as indicated and were infected with rLCMV i.c. 6 wk later, rLCMV memory mice containing helped or unhelped bT_{RM} were treated with anti-CD8a depleting antibody and challenged with LCMVwt i.c. (G) numbers of bT_{RM} ($CD8^+CD44^+CD69^+$) and (H) frequencies of T_M cells ($CD127^+KLRG1^-$) among bT_{RM} ($CD8^+CD44^+CD69^+$) were determined by flow cytometry in unchallenged rLCMV memory mice. (I–L) 6 wk after antibody-mediated depletion of $CD4^+$ T cells, rLCMV memory mice, as in F, were challenged with LCMVwt i.c. and analyzed 3 d later. (I) Quantification of $CD8^+$ T cells by immunohistochemistry. (J) Representative images of brain sections immunostained for CD8 (top, arrows) or LCMV (bottom). (G–I) Each symbol represents an individual mouse and bars indicate mean. Quantification of (K) $LCMV^+$ cells by immunohistochemistry (L) LCMV RNA by qPCR (normalized to naive mice infected with LCMVwt i.c. = 1) 3 d after LCMVwt i.c. challenge. Data represent mean + SEM (where included).

up-regulated GzmB (96 ± 1%) and Ki-67 (42 ± 3%) during i.c. challenge with LCMV-NP_{N400S} (unpublished data).

bT_{RM}–mediated rapid viral clearance depends on IFN-γ and perforin

T cell–mediated viral clearance from the brain can be achieved by cytolytic, i.e., perforin or Fas-dependent mechanisms, as well as by noncytolytic, cytokine-dependent pathways (Griffin, 2003; Pinschewer et al., 2010; Herz et al., 2015). To investigate cytokine production and cytotoxic potential of bT_{RM}, we depleted memory mice of circulating $CD8^+$ T cells and challenged them with LCMVwt i.c. (Fig. 8 A). We analyzed CD107a surface exposure as indicator of degranulation of cytotoxic granule release and production of IL-2, IFN-γ, and TNF upon in vitro peptide stimulation (Fig. 8 B and not depicted). In the absence of LCMVwt challenge and without peptide restimulation, bT_{RM} did not spontaneously produce detectable amounts of cytokines and did not degranulate. After LCMVwt i.c. challenge, bT_{RM} exhibitedIFN-γ production (9.7 ± 1.5%) and surface exposure of CD107a (9.0 ± 0.5%) in the absence of further ex vivo stimulation. After peptide stimulation, most bT_{RM} produced high amounts of IFN-γ in combination with surface exposure of CD107a, which was significantly higher in bT_{RM} from LCMVwt i.c. challenged animals (59.0 ± 2.4%) than from unchallenged controls (36.4 ± 3.1%; Fig. 8 B). In contrast, we detected comparably few bT_{RM} that coproduced IL-2 or TNF, and we failed to detect expression of FasL on bT_{RM} (unpublished data). Thus our analysis identified IFN-γ–producing bT_{RM} with cytotoxic granule release as main effector cell population after LCMVwt i.c. challenge.

Considering IFN-γ as the main effector cytokine expressed by bT_{RM}, we next tested bT_{RM} function in IFN-γ knockout (GKO) mice. Of note, IFN-γ is dispensable for the clearance of primary infection with attenuated rLCMV (Pinschewer et al., 2010) and bT_{RM} generation was not impaired in GKO mice (Fig. 8 C). We depleted circulating $CD8^+$ T cells in IFN-γ–deficient (GKO) and IFN-γ competent (control) rLCMV memory mice and subsequently challenged them with LCMVwt i.c. (Fig. 8, D–G). Before LCMVwt i.c. challenge, GKO rLCMV memory mice displayed slightly higher bT_{RM} numbers, but the fold expansion of bT_{RM} after virus challenge was similar in GKO and control animals (Fig. 8, D and E). This indicated that the cell-intrinsic reactivation capacity of bT_{RM} was unimpaired in GKO mice. Conversely, the number of infected cells (Fig. 8, D and F) and LCMV RNA loads (Fig. 8 G) 3 d after LCMVwt i.c. challenge were significantly higher in GKO memory mice than in control memory mice.

Based on the notion that bT_{RM} up-regulated the cytotoxic effector molecule Granzyme B after LCMV i.c. challenge (Fig. 7, G and H), we next investigated whether cytolytic effector functions (Kägi et al., 1994) contributed to bT_{RM}–mediated virus clearance. We thus generated perforin-deficient (PKO) rLCMV memory mice and depleted circulating $CD8^+$ T cells (Fig. 8, H–M), as before (Fig. 8 A). Perforin was dispensable for the generation of bT_{RM} (Fig. 8 H). Furthermore, after LCMVwt i.c. challenge, perforin-deficient bT_{RM} showed unimpaired up-regulation of Granzyme B (Fig. 8 I) and secondary expansion (Fig. 8, J and K). Nevertheless, PKO memory mice exhibited significantly higher numbers of infected cells (Fig. 8, J and L) and increased viral RNA loads (Fig. 8 M) than control memory mice. This demonstrated that bT_{RM} cells exert rapid IFN-γ production and perforin-dependent cytotoxicity, both of which made essential contributions to the rapid control of viral infection in the brain.

bT_{RM} cells protect from fatal immunopathological CNS disease in an antigen-dependent manner

i.c. infection of naive immunocompetent mice with LCMVwt results in fatal choriomeningitis, which is the result of antiviral $CD8^+$ T cell–mediated immunopathology (Cole et al., 1972). T_{RM} have been shown to amplify immune responses in nonlymphoid tissues during rechallenge with cognate antigen (Schenkel et al., 2013, 2014a). Here, we observed analogous findings in the brain (Fig. 4 B), raising the possibility that bT_{RM} could enhance immunopathological consequences of brain virus infection (Oehen et al., 1991). We therefore investigated how the presence of bT_{RM} impacts the disease after LCMVwt i.c. challenge. For that, we depleted LCMV-specific circulating T_M in rLCMV memory mice using anti-CD8 antibody 6 wk before LCMVwt i.c. challenge (Fig. 9 A). This timing enabled the reconstitution of the peripheral compartment with naive $CD8^+$ T cells before LCMVwt challenge (unpublished data). Analogous to the experiment in which anti-CD8 depletion and challenge had been performed simultaneously (Fig. 4, B and D), the presence of bT_{RM} resulted in enhanced T cell numbers in the brain when circulating memory $CD8^+$ T cells were present (Fig. 9, B and C). However, irrespective of the presence or absence of circulating memory $CD8^+$ T cells, brain LCMV loads as assessed 3 d after LCMVwt i.c. challenge were significantly reduced in mice with bT_{RM} compared with mice with only circulating T_M (Fig. 9, B, D, and E). As expected (Oehen et al., 1991), mice with only circulating T_M did not develop disease, demonstrating that the observed peripheral virus-specific T_M recall response can afford antiviral protection (Fig. 9 F). Furthermore, circulating T_M–depleted rLCMV memory mice without bT_{RM} developed fatal choriomenigitis, which had kinetics comparable to unimmunized control mice. Most importantly, six out of seven rLCMV memory

(B–E) n = 5 mice per group, (G–H) n = 4 mice per group, (I–L) n = 3 mice for naive WT mice infected with LCMVwt i.c. (white bars), n = 5–6 mice per group of rLCMV memory mice after LCMVwt i.c. challenge. *, $P < 0.05$; **, $P < 0.01$, one-way ANOVA with Tukey's multiple comparison test. One experiment was performed. Bars: 100 µm; (inset) 20 µm.

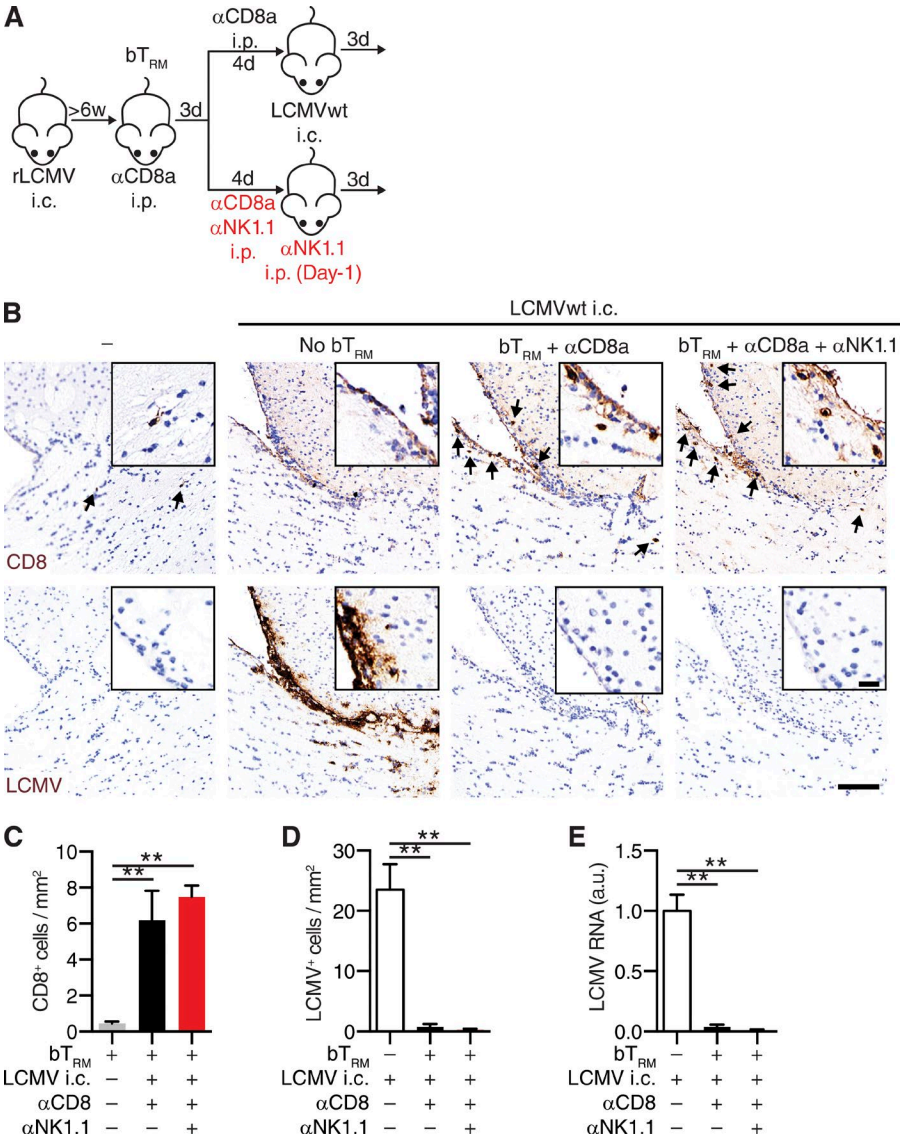

Figure 6. **bT$_{RM}$–mediated rapid viral clearance is independent of circulating NK cells.** (A) WT mice were infected with rLCMV i.c. 12 wk later, mice were treated with anti-CD8a only or in combination with anti-NK1.1 depleting antibody i.p., and subsequently challenged with LCMVwt i.c. Naive WT mice infected with LCMVwt i.c. were used as controls. Brains were analyzed 3 d after i.c. challenge. (B) Representative images of brain sections immunostained for CD8 (top, arrows) or LCMV (bottom). Bars: 100 µm; (inset) 20 µm. Quantification of CD8$^+$ T cells (C), LCMV$^+$ cells (D), or LCMV RNA by qPCR (E; normalized to naive mice infected with LCMVwt i.c. = 1). Data represent mean + SEM (n = 5 mice per group). **, $P < 0.01$, one-way ANOVA with Tukey's multiple comparison test. One experiment was performed.

mice with bT$_{RM}$ were protected from disease even though circulating T$_M$ cells had been depleted. This underscored the self-sufficient nature of bT$_{RM}$-mediated antiviral protection. Next, we investigated whether bystander activation of bT$_{RM}$ (Fig. 7) was sufficient to protect animals from fatal immunopathology. We therefore depleted rLCMV memory mice of circulating T$_M$ and challenged them with either LCMVwt or LCMV-NP$_{N400S}$ i.c. after reconstitution of circulating CD8$^+$ T cells. As expected, mice challenged with LCMV-NP$_{N400S}$ i.c. did not mount a D^b-NP$_{396-404}$–specific CD8$^+$ T cell response, but developed a CD8$^+$ T cell response specific for the D^b-GP$_{33-41}$ epitope (data not shown), to which they had not been previously exposed (rLCMV does not encode for LCMV-GP$_{33-41}$). Unlike rLCMV memory mice challenged with LCMVwt i.c., challenge with LCMV-NP$_{N400S}$ i.c. resulted in the development of fatal choriomeningitis with disease kinetics comparable to unimmunized control mice (Fig. 9 G). Altogether, this demonstrated that bT$_{RM}$ immunity was antigen-specific and provided rapid autonomous elimination of virus-infected cells from the brain and thereby protected from fatal immunopathological disease.

DISCUSSION

The identification of T$_{RM}$ as a separate lineage of long-lived memory T cells has fundamentally reshaped our concepts of cell-mediated immunity to infection. With this study, we establish bT$_{RM}$ as an autonomous first line of adaptive immune defense against viral infection of the brain. bT$_{RM}$ were found after acute infection with rLCMV or a replication-deficient modified vaccinia virus strain in mice, attesting to the general validity of our findings. bT$_{RM}$ showed strong proliferative potential and protected against fatal viral infection in an organ-autonomous manner, independent of the recruitment of circulating CD8$^+$ memory T cells.

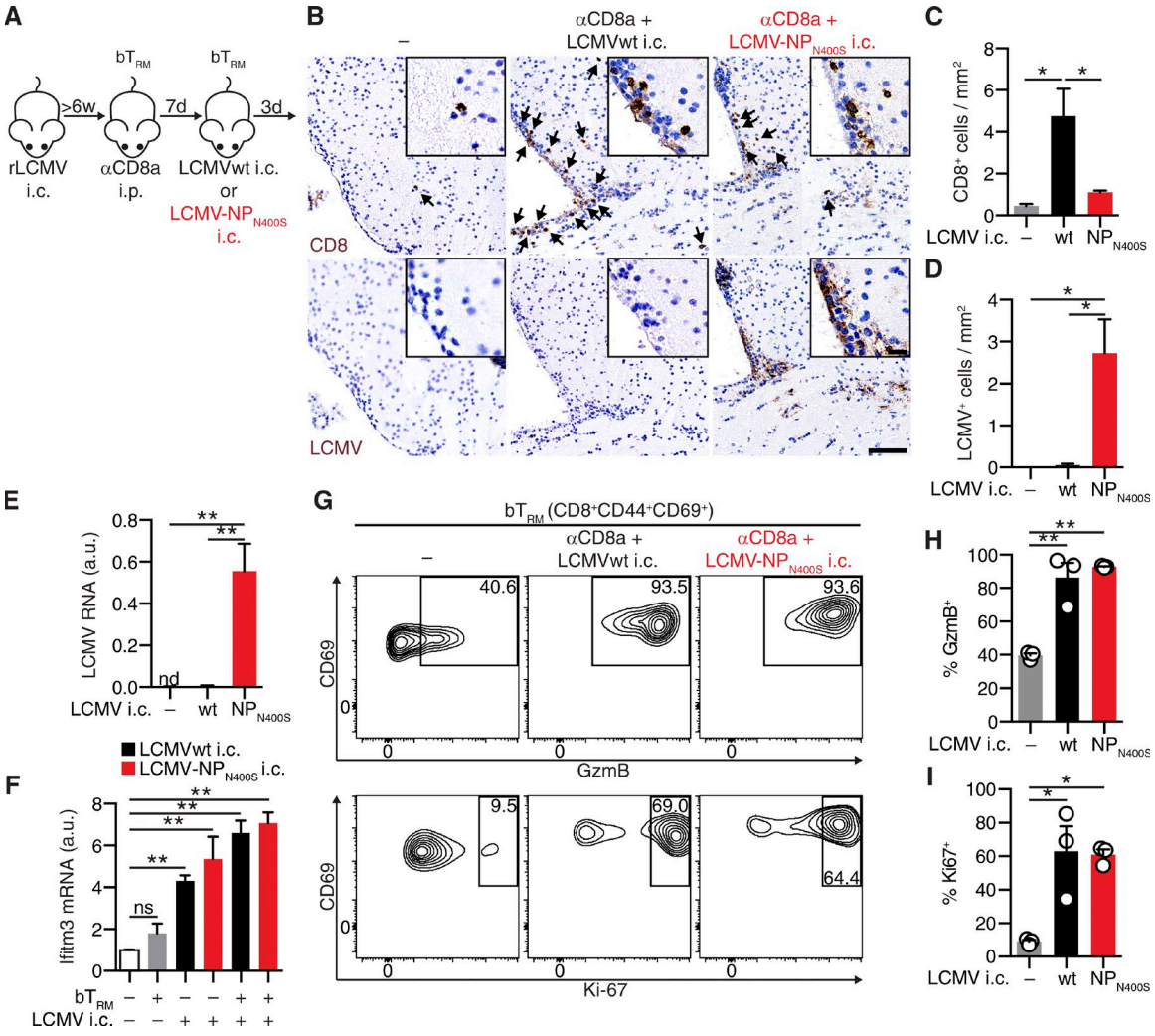

Figure 7. **MHC-I–restricted presentation of cognate antigen is required for bT_{RM}–mediated virus clearance.** (A) WT mice were infected with rLCMV i.c. to generate bT_{RM}. At least 6 wk later, mice were treated with anti-CD8a depleting antibody i.p. before i.c. challenge with LCMVwt or LCMV-NP_{N400S} or left unchallenged. Brains were analyzed 3 d later. (B) Representative images of CD8 (top, arrows) or LCMV (bottom) on brain sections of virus challenged or unchallenged (–) mice. Bars: 100 µm; (inset) 20 µm. Quantification of $CD8^+$ T cells (C), $LCMV^+$ cells (D), or LCMV RNA by qPCR (E; normalized to naive mice infected with LCMV i.c. = 1). (F) Quantification of *Ifitm3* mRNA by qPCR in the brain of mice in relation to the presence of bT_{RM} (+) and LCMVwt or LCMV-NP_{N400S} i.c. infection (+; normalized to uninfected mice = 1). (G) Representative flow cytometry plot of GzmB and Ki-67–expressing bT_{RM} ($CD8^+CD44^+CD69^+$). Numbers represent frequencies of positive cells. Frequencies of (H) GzmB and (I) Ki-67–expressing bT_{RM}. (H and I) Each symbol represents an individual mouse. Data represent mean + SEM (n = 3–5 mice per group). *, $P < 0.05$; **, $P < 0.01$, one-way ANOVA followed by Tukey's (C, D, E, H, and I) or Dunnet's multiple comparison test (F). One representative out of two independent experiments is shown (B–I).

Similar to other nonlymphoid organs (Steinert et al., 2015), $CD69^+$ bT_{RM} represented 90% of $CD8^+$ T cells in the brain. Contrary to brain infection with vesicular stomatitis virus (Wakim et al., 2010), we found in two independent models that CD103 was expressed only on a proportion of bT_{RM}. This may be a result of differences in isolation and quantification methods, as has been described for other organs (Steinert et al., 2015). We do not exclude the possibility that $CD103^+$ and $CD103^-$ bT_{RM} may be functionally different; however both subsets persisted in stable proportions over time, exhibited an analogous preference for retention at surface-lining structures of the brain, and showed equal proliferative capacity upon reactivation. Although bT_{RM} show very limited survival and proliferative capacity in vitro (Wakim et al., 2010), they seem to possess self-renewing capacity in vivo and exhibit high proliferative capacity after reactivation. Similar to central memory T cells (Burchill et al., 2003; Willinger et al., 2005; Hand et al., 2010), the population of long-lived bT_{RM} seems to be maintained by Stat5-driven homeostatic proliferation, preferentially at brain surface structures, such as meninges and periventricular areas. However, the exact nature of a supposed T_{RM} maintaining microenvironment near

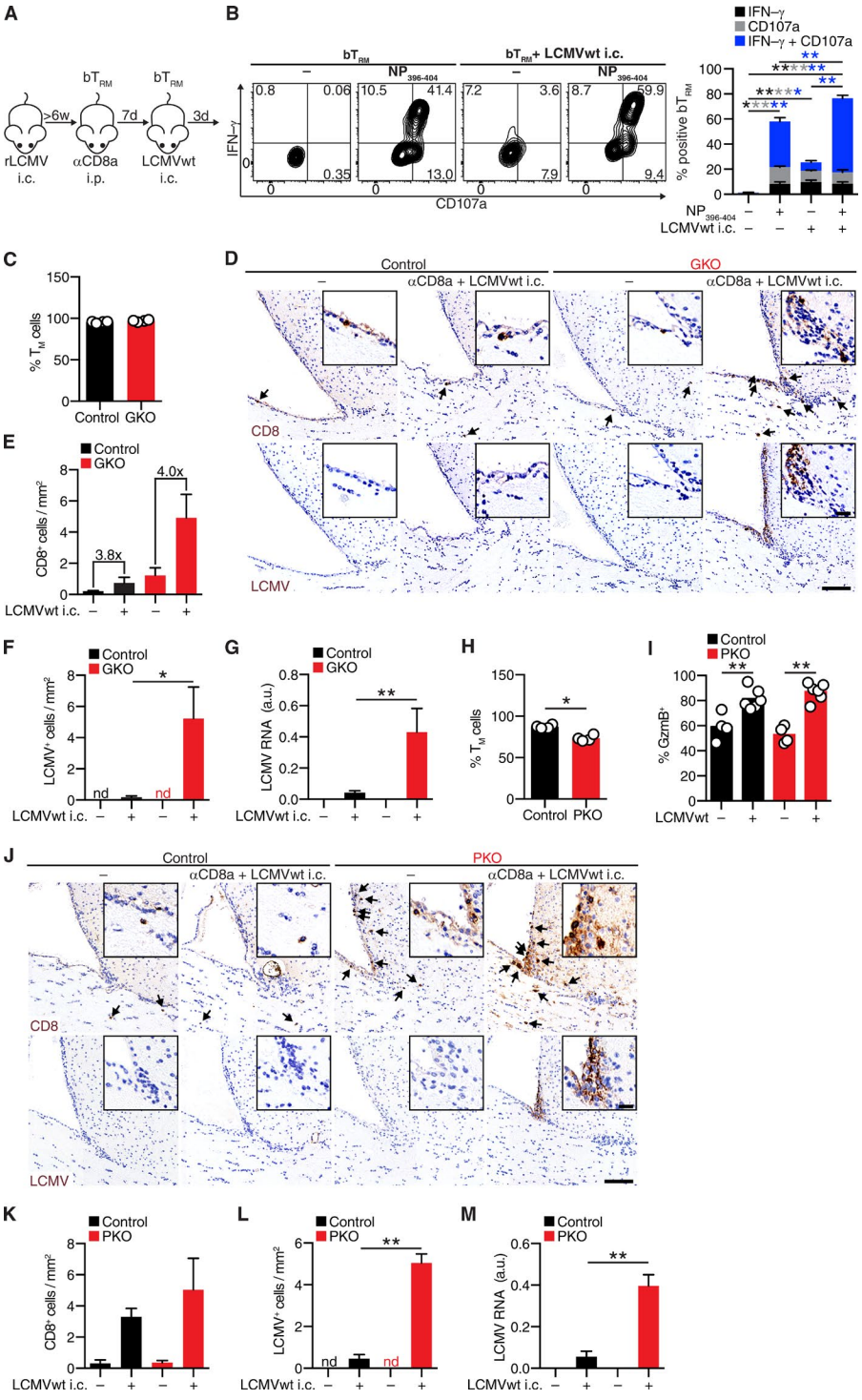

Figure 8. **bT_{RM}–mediated rapid virus clearance depends on IFN-γ and perforin.** (A) Mice were infected with rLCMV i.c to generate bT_{RM}. At least 6 wk later, mice were treated with anti-CD8a depleting antibody i.p. before LCMVwt i.c. challenge or left unchallenged. Brains were analyzed 3 d later. (B, left) Representative flow cytometry plot of IFN-γ production and degranulation as measured by surface exposure of CD107a in bT_{RM} ($CD8^+CD44^+CD69^+$) of unchallenged (bT_{RM}) or LCMVwt i.c.-challenged (bT_{RM} + LCMVwt i.c.) WT mice with (+) or without (–) in vitro $NP_{396-404}$ peptide stimulation. Numbers indicate frequencies (%) of cells in corresponding gates. (right) Frequencies (mean + SEM) of IFN-γ–positive (black bars), CD107a positive (gray bars), and double-positive (blue bars) bT_{RM} with (+) or without (–) LCMVwt i.c. challenge and with (+) or without (–) in vitro $NP_{396-404}$ peptide stimulation (n = 3–4 mice per group). (C–G) IFN-γ–competent (control)- or GKO-rLCMV memory mice were generated and treated as in A. (C) Frequencies of T_M cells ($CD127^+KLRG1^-$) among bT_{RM} ($CD8^+CD44^+CD69^+$) as determined by flow cytometry in unchallenged IFN-γ–competent (control) and GKO mice. Each symbol represents an individual mouse and bars indicate mean (n = 4 mice per group). (D) Representative images of immunostained brain sections for CD8 (top, arrows) or LCMV (bottom). (E) Quantification of $CD8^+$ T cells, (F) $LCMV^+$ cells, or (G) LCMV RNA by qPCR (normalized to naive mice infected with LCMVwt i.c. = 1) in brains of GKO and control mice with (+) or without (–) LCMVwt i.c. challenge. Data represent mean + SEM (n = 3–10 mice per group). (H–M) Perforin-competent (control)- or PKO-rLCMV memory mice were generated and treated as in A. (H) Frequencies of T_M cells among bT_{RM} (as in C) in unchallenged perforin-competent (control) and PKO mice. Each symbol represents an individual mouse and bars indicate mean (n = 4 mice per group). (I) Frequencies of GzmB-expressing cells among bT_{RM} as determined by flow cytometry 3 d after LCMVwt i.c. challenge of control or PKO mice. Each symbol represents an individual mouse, and bars indicate mean (n = 4–6 mice per group). (J) Representative images of immunostained brain sections for CD8 (top, arrows) or LCMV (bottom). (K) Quantification of $CD8^+$ T cells, (L) $LCMV^+$ cells, or (M) LCMV RNA by qPCR (normalized to naive mice infected with LCMVwt i.c. = 1) in brains of PKO and control mice with (+) or without (–) LCMVwt i.c. challenge. Data represent mean + SEM (n = 4–6 mice per group). *, $P < 0.05$; **, $P < 0.01$, asterisk colors represent multiple comparisons performed, two-way ANOVA with Tukey's multiple comparisons (B), one way ANOVA with Sidak's multiple comparisons test (I), unpaired two-tailed Student's t test (C, F, G, H, L, and M). One representative (B–F and J–M) or pool (G) of two independent experiments is shown. (H and I) Experiments were performed once. Bars, 100 µm; (inset) 20 µm.

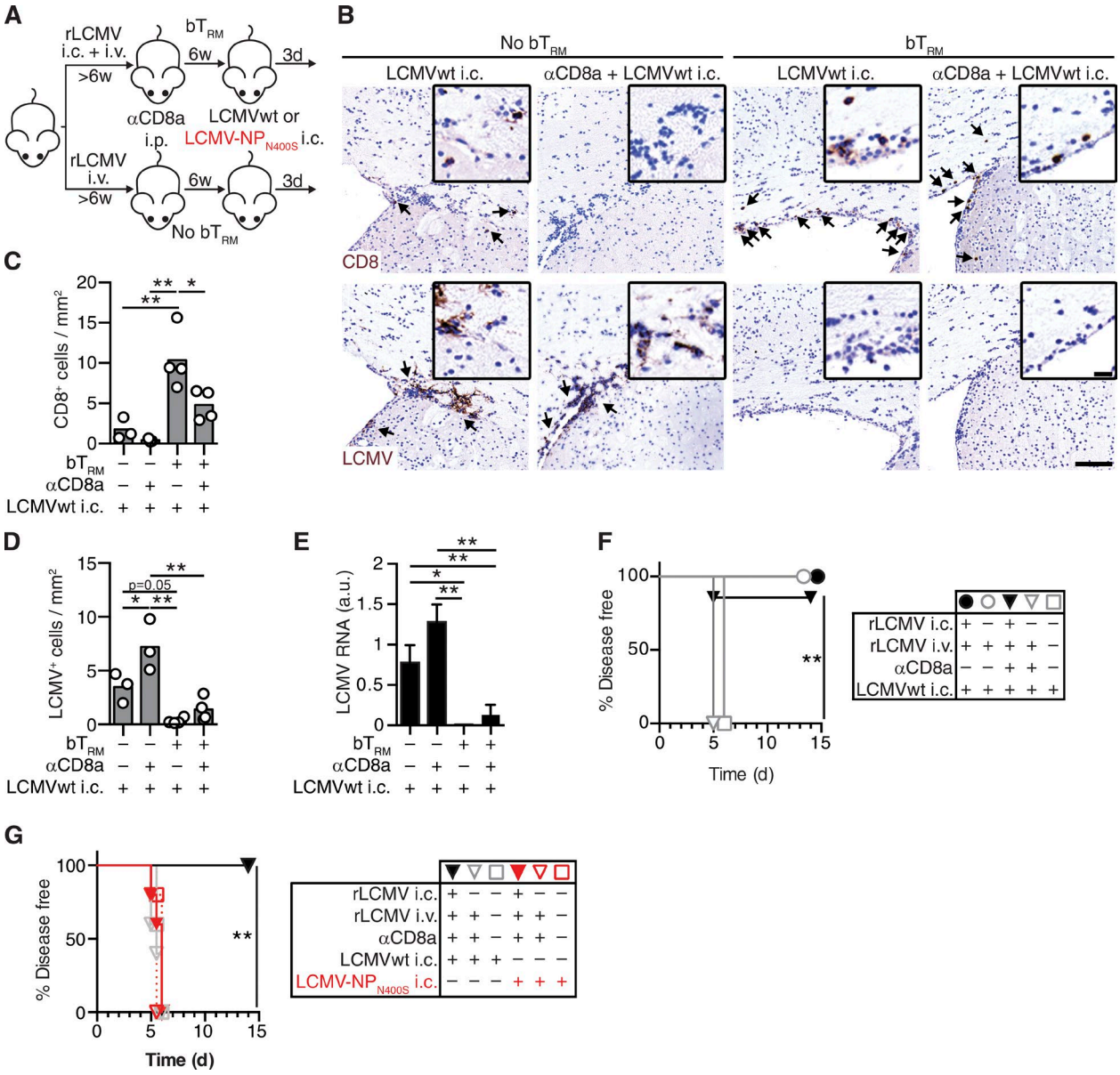

Figure 9. **bT_{RM} protect against LCMV-induced choriomeningitis in an antigen-dependent manner.** (A) WT mice were infected with rLCMV i.v. (no bT_{RM}) or i.v. + i.c. (bT_{RM}). At least 6 wk later, mice were treated with anti-CD8a-depleting antibody i.p. followed by 6 wk reconstitution of naive $CD8^+$ T cells. Subsequently mice were challenged with LCMVwt or LCMV-NP_{N400S} i.c. (B) Representative images of CD8 (top, arrows) or LCMV (bottom, arrow) on brain sections 3 d after LCMVwt i.c. challenge. Bars: 100 µm; (inset) 20 µm. (C) Quantification of $CD8^+$ T cells and (D) $LCMV^+$ cells of mice as in C. Each symbol represents an individual mouse and bars indicate mean (n = 3–4 mice per group). (E) LCMV RNA by qPCR (normalized to naive mice infected with LCMV i.c. = 1) of mice as in C. Data represent mean + SEM (n = 3–4 mice per group). (F) Incidence of fatal choriomenigitis after LCMVwt i.c. challenge (n = 7–8 mice per group). (G) Incidence of disease after LCMVwt or LCMV-NP_{N400S} i.c. challenge (n = 5 mice per group). *, $P < 0.05$; **, $P < 0.01$, (C–E) one-way ANOVA with Sidak's multiple comparisons test, (F and G) Log rank Mantel-Cox test. (C, D, E, and G) Experiments were performed once. (F) Data are pooled from two independent experiments.

tissue surfaces that was also observed in other organs, i.e., in the skin (Gebhardt et al., 2009), remains to be investigated.

In naive hosts, the task of rapidly detecting invading pathogens and alerting the adaptive immune defense generally falls to the innate immune system (Iwasaki and Medzhitov, 2015). The resulting secretion of antiviral effector cytokines, such as type I interferons, is crucial to limiting virus spread until adaptive immune responses are induced and can accomplish viral clearance (McNab et al., 2015). T_{RM} from peripheral organs other than the brain have been described to subserve a similar immunological function, i.e., to alert circulating T cell subsets to invading pathogens and to induce

antiviral genes in the tissue surrounding the site of initial infection (Ariotti et al., 2014; Schenkel et al., 2014a). These functions were reported to be largely dependent on inflammatory cytokines, such as IFN-γ. Similar to T_{RM} from other organs, we show here that bT_{RM} share the capacity to secrete IFN-γ upon antigen reencounter. However, they largely do that in combination with the release of cytotoxic granules, and perforin-mediated cytotoxicity was essential for rapid bT_{RM}-mediated virus control. One may thus speculate that IFN-γ–deficient bT_{RM} fail to provide sufficient noncytolytic antiviral function, or fail to prepare the site of infection for lytic effector function as a result of impaired up-regulation of MHC I expression on infected cells (Bergmann et al., 2003). Whereas both possibilities are not mutually exclusive and can contribute to the observed outcome, our data strongly suggest that a direct interaction of bT_{RM} with infected cells rather than a generalized antiinflammatory state is necessary for bT_{RM}-mediated rapid viral elimination. This conclusion is based on our observation that bT_{RM} can be activated in a bystander manner, i.e., in the absence of cognate antigen and solely as the result of the inflammatory environment (Kohlmeier et al., 2010; Soudja et al., 2012; Raué et al., 2013), yet under such circumstances fail to rapidly control the virus. This does not, however, exclude the possibility that bystander activation may contribute to a viral load reduction in the brain. Furthermore, depending on the pathogen type and infection scenario, bT_{RM}-driven induction of IFN-γ response genes may be sufficient to limit early pathogen spread or even to cleanse viruses from nonrenewable cells such as neurons (Griffin, 2003; Herz et al., 2015).

Neurotropic viruses of hematogenous origin frequently infect the CNS secondary to systemic infection. Neuroinvasion typically occurs through the brains outer or inner linings (McGavern and Kang, 2011), namely the meninges or the ependyma, to subsequently spread into the brain parenchyma. The resulting inflammation manifests as meningitis or even encephalitis and can be life-threatening (Gilden et al., 2007). Our model of intracranial rLCMV immunization recapitulates the spread from the brain linings into the parenchyma albeit it does not reproduce neuroinvasion secondary to systemic infection. Conversely, its attenuated behavior enabled us to study solid bT_{RM} immunity without the caveats of life-threatening complications from primary brain infection.

Although we noted a protective function of bT_{RM} in infection, T_{RM}–mediated activation and recruitment of inflammatory cells to the site of infection can, however, also have detrimental effects such as those described in the context of skin contact hypersensitivity (Gaide et al., 2015). In organs with limited regenerative capacity, such as the CNS, excessive inflammation can induce collateral damage (immunopathology). In this regard, severe immunopathological disease is one of the most dangerous complications of viral infections in the brain, and depending on pathogen loads, circulating T_M can even accentuate disease rather than prevent it (Oehen et al., 1991). Therefore, not only infections of the CNS but also the resulting immune responses must be tightly controlled. The functioning of bT_{RM} as a border patrol, which rapidly detects and autonomously eliminates the first few virus-infected cells, thus bypasses the need for antigen drainage to lymph nodes and reactivation of T_M cells inside secondary lymphoid organs. It has been shown for other organs that T_{RM} cells use a continuous migratory behavior, enabling few cells to survey large organ structures and readily detect their cognate antigen (Ariotti et al., 2012). The positioning and preferential maintenance of bT_{RM} at surface-associated brain structures and in proximity to vessels as described in this study therefore matches the specific immunological challenge and need of the brain to limit viral spread from the circulation and brain linings into the parenchyma and to rapidly eliminate the initially infected cells. Thereby, bT_{RM} can balance pathogen control against excessive inflammation.

Based on the present observations, we propose to adapt the concept of immunological privilege of the brain. With identification of the bT_{RM} compartment, the brain undoubtedly maintains powerful immunological forces to fight recurrent microbial intruders. This observation stands in stark contrast to the several layers of immunomodulatory mechanisms, including constitutively low expression of MHC molecules (Neumann et al., 1995), which are in place to limit inflammation in the brain (Galea et al., 2007). Thus, pathogens that have previously invaded the brain appear to be specifically excluded from this immunological privilege and are instead rapidly and efficiently eliminated by bT_{RM}. It is tempting to speculate that bT_{RM} immunity must be particularly potent because the blood–brain barrier prevents antibody access to the brain, and thus is largely excluding this organ from protection by the humoral arm of immunological memory.

MATERIALS AND METHODS

Mice. C57BL/6 WT, IFN-γ deficient (GKO; Dalton et al., 1993), perforin-deficient (PKO; Kägi et al., 1994), OT-1 TCR transgenic (Hogquist et al., 1994), and P14 TCR (Pircher et al., 1989) transgenic mice were bred and lodged under P2 conditions in the animal facilities of the University Medical Centre of Geneva and Munich. Sex- and age-matched mice between 6 and 12 wk of age were used for experiments. All animal experiments were authorized by the cantonal veterinary office of Geneva and performed in agreement with the Swiss law for animal protection.

Virus infection. Recombinant LCMV strains were generated according to established methods (Pinschewer et al., 2003). The following virus strains were used: recombinant LCMV encoding for the glycoprotein of vesicular stomatitis virus (VSV) instead of its own glycoprotein (rLCMV/INDG, abbreviated rLCMV throughout); rLCMV encoding for a chimeric glycoprotein of VSV containing the leader sequence of LCMV glycoprotein with the GP33 epitope of LCMV (rLCMV-GP33); and recombinant LCMV encoding for OVA (rLCMV-OVA). Genetically engineered WT

LCMV (LCMVwt, Armstrong strain) and LCMV mutant virus (LCMV-NP_{N400S}) lacking the CTL-specific epitope $NP_{396-404}$ were generated as described previously (Johnson et al., 2015). Viruses were produced, titrated, and administered to mice as previously described (Flatz et al., 2006). For transient virus infection in the brain, 10^4 PFU rLCMV was administered i.c. i.v. infected control animals were injected i.c. with vehicle. Memory and naive mice were challenged with 10^3 PFU LCMVwt (Armstrong strain) i.c. Incidence of choriomenigitis was determined by occurrence of general malaise and hind limb cramps, and severely diseased animals were immediately sacrificed. Brain virus load was analyzed by quantitative RT-PCR for LCMV-NP (McCausland and Crotty, 2008). Brain total RNA was isolated from deparaffinized tissue sections using RNeasy Mini kit (QIAGEN), cDNA was synthesized using iScript cDNA synthesis kit (Bio-Rad Laboratories), and relative expression of LCMV S segment was determined against GAPDH as housekeeping gene (QIAGEN) using iQ SYBR Green Supermix (Bio-Rad Laboratories).

Replication-deficient MVA-OVA was generated as described previously (Staib et al., 2004). 2×10^6 IU MVA-OVA was administered intrathecally (i.th.) as previously described (Rothhammer et al., 2014). In some experiments, OT-1 or P14TCR transgenic $CD8^+$ T cells were adoptively transferred into naive C57BL/6 mice 24 h before i.c. or i.th. infection.

Antibody-mediated depletion. For depletion of peripheral $CD4^+$ T cells, $CD8^+$ T cells, or NK cells, mice were treated i.p. twice over a 3-d interval with 250 µg anti-CD4 antibody (YTS191), 450 µg anti-CD8a depleting antibody (clone YTS169.4), or 500 µg anti-NK1.1 depleting antibody (clone PK136), respectively. Depletion of T cells or NK cells was confirmed by flow cytometry showing T cell or NK cell frequencies <0.1% during LCMVwt i.c. challenge. After antibody-mediated $CD8^+$ T cell depletion and subsequent reconstitution by naive $CD8^+$ T cells, frequencies of D^b-$NP_{396-404}$–specific $CD8^+$ T cells in rLCMV memory mice were reduced from 1.4 ± 0.3% to 0.06 ± 0.02%, which was not significantly above technical background in uninfected naive control mice (0.005 ± 0.004%).

Intravascular staining of $CD8^+$ T cells. Mice were injected i.v. with 3 µg PE-labeled anti-CD8b (YTS156.7.7) according to previously described protocols (Anderson et al., 2014). 3 min later, peripheral blood samples were taken, and mice were anesthetized and perfused with PBS. Brains were dissected and processed immediately (<10 min after antibody injection) for leukocyte isolation (see Flow cytometry).

Immunohistochemistry. For immunohistochemical bright field staining of mouse tissue, brains and spleen were prepared and fixed in Hepes-glutamic acid buffer-mediated organic solvent protection effect (HOPE, DCS Innovative) fixative as previously described (Bergthaler et al., 2007) and embedded in paraffin. Upon inactivation of endogenous peroxidases, tissue sections were incubated with rat anti–mouse CD8a (YTS169.4) or rat anti-LCMV NP (VL-4; Battegay et al., 1991). Bound primary antibodies were visualized with biotin-labeled anti–rat antibody and streptavidin-peroxidase staining method using polymerized 3,3′-diaminobenzidine (all reagents from Dako; haemalaun counterstaining of nuclei).

For immunofluorescence staining of mouse tissue, cryosections were fixed with 2% PFA for 5 min and unspecific binding blocked (PBS/1% BSA/2% FCS). Sections were incubated with FITC-labeled Armenian hamster anti–mouse CD103 (2E7) and rat anti–mouse CD8a (YTS169.4), followed by rabbit anti-FITC (Invitrogen) antibody. Bound antibodies were visualized with Alexa Fluor 488–labeled goat anti–rabbit and Cy3-labeled goat anti–rat secondary antibodies (Jackson ImmunoResearch Laboratories). Nuclei were stained with DAPI (Invitrogen).

For immunofluorescence staining of paraffin embedded tissue, mice were transcardially perfused with 4% PFA. After antigen retrieval and unspecific binding blocking (PBS/10% FCS), sections were incubated with rat anti–human CD3 (CD3-12), rat anti–mouse CD8 (clone 4SM15), goat anti–mouse CD69 (AF2386), rabbit anti-VWF (ab6994), rabbit anti–Ki-67 (ab66155), and rabbit anti–phospho-Stat5 (tyr694, C71E5). Bound antibodies were visualized with Alexa Fluor 488 or Alexa Fluor 568 goat anti–rabbit tyramide signal (TSA) amplification (Thermo Fisher Scientific), Cy2- or Cy3-labeled goat-anti–rat, or Cy5-labeled goat anti–rabbit secondary antibodies (Jackson ImmunoResearch Laboratories). Nuclei were stained with DAPI (Invitrogen).

Immunostained sections were scanned using Pannoramic Digital Slide Scanner 250 FLASH II (3DHISTECH) in 200× magnification. Quantifications were performed manually using Pannoramic Viewer software (3DHISTECH) blinded to the experimental setup of histological samples. For representative images, white balance was adjusted and contrast was linearly enhanced using the tools levels, curves, brightness, and contrast in Photoshop CS6 (Adobe). For histocytometry analysis, fluorescence-immunostained brain sections were scanned using a high-dynamic range camera (16 bit).

For histocytometry and density plots, $CD3^+$ or $CD8^+$ cells, respectively, were detected on scanned slides applying a custom-programmed script in Cognition Network Language (Definiens Developer XD software). For analysis of distance, a grayscale distance map was computed to encode the closest distance of each detected $CD3^+$ or $CD8^+$ cell to the brain surface and vessels (detected by von-Willebrand Factor staining) and mean values of distance maps were extracted. For histocytometry, each $CD3^+$ cell size (area), as well as mean and max grayscale values for CD3, P-Stat5, and DAPI signals, were extracted. The resulting CSV files were converted to .fcs format using an open source program (FlowJo). The converted file was analyzed using FlowJo X. Co-staining of anti-CD3 and anti–phospho-Stat5 was gated based on control staining without primary P-Stat5 antibody.

Flow cytometry. For staining, the following antibodies were used: anti–Bcl-2 (BCL/10C4), anti-CD3e (145-2C11), anti-CD8a (53–6.7), anti-CD11a (M17/4), anti-CD11b (M1/70), anti-CD44 (IM7), anti-CD45.1 (A20), anti-CD45.2 (104), anti-CD45R/B220 (RA3-6B2), anti-CD49a (HMα1), anti-CD49b (DX5), anti-CD49d (9C10), anti-CD69 (H1.2F3), anti-CD103 (2E7), anti-CD107a (1D4B), anti-CD127 (A7R34), anti–E-Cadherin (36/E-Cadherin), anti-FasL (MFL3), anti–Granzyme B (GB11), anti–IFN-γ (XMG1.2), anti–IL-2 (JES6-5H4), anti-Integrinβ7 (FIB27), anti–Ki-67 (SolA15), anti-KLRG1 (2F1), anti-NK1.1 (PK136), and anti-TNF (MP6-XT22). For detection of virus-specific $CD8^+$ T cells, D^b-$NP_{396–404}$-tetramer (TCmetrix) or K^b-$B8R_{20–27}$-tetramer (provided by D.H. Busch, Institute of Medical Microbiology, Immunology and Hygiene, Technical University Munich, Munich, Germany) were used.

Peripheral blood samples and splenocytes were collected in FACS-Buffer (10% FCS, 10 mM EDTA, and 0.01% NaN_3 in PBS). Peripheral blood erythrocytes were lysed using BD FACS lysing solution (BD). For the preparation of brain leukocytes, mice were anesthetized and transcardially perfused with PBS. Brains were minced, digested with Collagenase/DNaseI (Roche), and homogenized using 70-µm cell strainers (BD). Leukocytes were separated using a discontinuous Percoll gradient (30%/70%). Surface staining was performed with directly labeled antibodies and tetramers in FACS buffer. Isolated $CD8^+$ T cell numbers were quantified using TruCOUNT tubes (BD) or AccuCheck Counting Beads (Invitrogen) as previously described (Steinbach et al., 2013). Intracellular staining of Ki-67 was performed using FoxP3/Transcription Factor Staining Buffer Set (eBioscience) according to manufacturer's instructions. For ex vivo staining of Granzyme B, cells were fixed and permeabilized using commercial permeabilization buffer set (BioLegend). To assess degranulation and intracellular cytokine production, brain leukocytes were cultured for 5 h in the presence of 5 µg/ml FITC-labeled anti-CD107a antibody, monensin, and brefeldin A. Cells were stimulated in vitro with 1 µM $NP_{396–404}$ peptide or left unstimulated, respectively. Cells were harvested and dead cells were excluded from the analysis using Zombie NIR Fixable Viability kit (BioLegend). Cells were fixed and permeabilized using commercial permeabilization buffer set (BioLegend), followed by intracellular staining for cytokines, respectively. Flow cytometric samples were acquired on a Gallios cytometer (Beckman-Coulter) equipped with three lasers (blue, 488 nm; red, 633 nm; and violet, 405 nm) using appropriate filter sets and compensation controls. Gates were assigned according to appropriate control populations. A CyAn ADP analyzer (Beckman-Coulter) was used for experiments involving MVA-OVA.

Statistical analysis. Analysis was performed using GraphPad 6.0 (Prism). To assess significant differences between single measurements of two groups, unpaired or paired two-tailed Student's *t* test was used, whereas differences between single measurements of more than two groups was assessed by one-way ANOVA, followed by post hoc analyses of selected pairs of datasets using Sidak's multiple comparisons test or all pairs of datasets using Tukey's multiple comparisons test to control for multiple comparisons. To assess significant differences between groups with multiple measurements, two-way repeated-measures ANOVA was performed followed by Dunnet's multiple comparisons test against control group. For comparison of disease incidence, Log rank (Mantel-Cox) test was used. $P < 0.05$ was considered significant, and $P < 0.01$ was considered highly significant, whereas $P > 0.05$ was considered statistically not significant.

Online supplemental material. Fig. S1 shows the gating strategy used for analysis of brain-derived leukocytes. Fig. S2 shows the histocytometry data processing and the gating strategy. Online supplemental material is available at http://www.jem.org/cgi/content/full/jem.20151916/DC1.

ACKNOWLEDGMENTS

We thank Prof. D.H. Busch (Technical University Munich) for providing K^b/B8R20 tetramers.

D. Merkler holds stipendiary professorships of the Swiss National Science Foundation (No. PP00P3_152928) and is supported by the Klaus-Tschira Foundation, Helmut Horten Foundation, and Gebert-Rüf Foundation. D. Merkler, K. Steinbach, and N. Page are supported by the Swiss MS Society. T. Korn is funded by SyNergy, ERC consolidator grant, DFG SFB 1054, TR 128. I. Drexler is supported by Deutsche Forschungs Gesellschaft GRK 1949.

The authors declare no competing financial interests.

Author contributions: K. Steinbach and I. Vincenti performed the experiments and analyzed the data. M. Kreutzfeldt, N. Page, I. Wagner, and A. Muschaweckh assisted in mouse experiments, data collection, and analysis. D. Pinschewer and T. Korn were involved in study design. I. Drexler provided viral vector. K. Steinbach and D. Merkler designed the studies. K. Steinbach, D. Pinschewer, and D. Merkler wrote and revised the manuscript. All authors discussed results and commented on the manuscript.

Submitted: 10 December 2015

Accepted: 20 May 2016

REFERENCES

Adachi, T., T. Kobayashi, E. Sugihara, T. Yamada, K. Ikuta, S. Pittaluga, H. Saya, M. Amagai, and K. Nagao. 2015. Hair follicle-derived IL-7 and IL-15 mediate skin-resident memory T cell homeostasis and lymphoma. *Nat. Med.* 21:1272–1279. http://dx.doi.org/10.1038/nm.3962

Anderson, K.G., K. Mayer-Barber, H. Sung, L. Beura, B.R. James, J.J. Taylor, L. Qunaj, T.S. Griffith, V. Vezys, D.L. Barber, and D. Masopust. 2014. Intravascular staining for discrimination of vascular and tissue leukocytes. *Nat. Protoc.* 9:209–222. http://dx.doi.org/10.1038/nprot.2014.005

Ariotti, S., J.B. Beltman, G. Chodaczek, M.E. Hoekstra, A.E. van Beek, R. Gomez-Eerland, L. Ritsma, J. van Rheenen, A.F. Marée, T. Zal, et al. 2012. Tissue-resident memory $CD8^+$ T cells continuously patrol skin epithelia to quickly recognize local antigen. *Proc. Natl. Acad. Sci. USA.* 109:19739–19744. http://dx.doi.org/10.1073/pnas.1208927109

Ariotti, S., M.A. Hogenbirk, F.E. Dijkgraaf, L.L. Visser, M.E. Hoekstra, J.Y. Song, H. Jacobs, J.B. Haanen, and T.N. Schumacher. 2014. T cell memory. Skin-resident memory $CD8^+$ T cells trigger a state of tissue-wide pathogen alert. *Science.* 346:101–105. http://dx.doi.org/10.1126/science.1254803

Battegay, M., S. Cooper, A. Althage, J. Bänziger, H. Hengartner, and R.M. Zinkernagel. 1991. Quantification of lymphocytic choriomeningitis virus with an immunological focus assay in 24- or 96-well plates. *J. Virol. Methods.* 33:191–198. http://dx.doi.org/10.1016/0166-0934(91)90018-U

Bergmann, C.C., B. Parra, D.R. Hinton, R. Chandran, M. Morrison, and S.A. Stohlman. 2003. Perforin-mediated effector function within the central nervous system requires IFN-gamma-mediated MHC up-regulation. *J. Immunol.* 170:3204–3213. http://dx.doi.org/10.4049/jimmunol.170.6.3204

Bergsbaken, T., and M.J. Bevan. 2015. Proinflammatory microenvironments within the intestine regulate the differentiation of tissue-resident CD8$^+$ T cells responding to infection. *Nat. Immunol.* 16:406–414. http://dx.doi.org/10.1038/ni.3108

Bergthaler, A., D. Merkler, E. Horvath, L. Bestmann, and D.D. Pinschewer. 2007. Contributions of the lymphocytic choriomeningitis virus glycoprotein and polymerase to strain-specific differences in murine liver pathogenicity. *J. Gen. Virol.* 88:592–603. http://dx.doi.org/10.1099/vir.0.82428-0

Burchill, M.A., C.A. Goetz, M. Prlic, J.J. O'Neil, I.R. Harmon, S.J. Bensinger, L.A. Turka, P. Brennan, S.C. Jameson, and M.A. Farrar. 2003. Distinct effects of STAT5 activation on CD4$^+$ and CD8$^+$ T cell homeostasis: development of CD4$^+$CD25$^+$ regulatory T cells versus CD8$^+$ memory T cells. *J. Immunol.* 171:5853–5864. http://dx.doi.org/10.4049/jimmunol.171.11.5853

Carbone, F.R. 2015. Tissue-Resident Memory T Cells and Fixed Immune Surveillance in Nonlymphoid Organs. *J. Immunol.* 195:17–22. http://dx.doi.org/10.4049/jimmunol.1500515

Casey, K.A., K.A. Fraser, J.M. Schenkel, A. Moran, M.C. Abt, L.K. Beura, P.J. Lucas, D. Artis, E.J. Wherry, K. Hogquist, et al. 2012. Antigen-independent differentiation and maintenance of effector-like resident memory T cells in tissues. *J. Immunol.* 188:4866–4875. http://dx.doi.org/10.4049/jimmunol.1200402

Cole, G.A., N. Nathanson, and R.A. Prendergast. 1972. Requirement for theta-bearing cells in lymphocytic choriomeningitis virus-induced central nervous system disease. *Nature.* 238:335–337. http://dx.doi.org/10.1038/238335a0

Dalton, D.K., S. Pitts-Meek, S. Keshav, I.S. Figari, A. Bradley, and T.A. Stewart. 1993. Multiple defects of immune cell function in mice with disrupted interferon-gamma genes. *Science.* 259:1739–1742. http://dx.doi.org/10.1126/science.8456300

Flatz, L., A. Bergthaler, J.C. de la Torre, and D.D. Pinschewer. 2006. Recovery of an arenavirus entirely from RNA polymerase I/II-driven cDNA. *Proc. Natl. Acad. Sci. USA.* 103:4663–4668. http://dx.doi.org/10.1073/pnas.0600652103

Gaide, O., R.O. Emerson, X. Jiang, N. Gulati, S. Nizza, C. Desmarais, H. Robins, J.G. Krueger, R.A. Clark, and T.S. Kupper. 2015. Common clonal origin of central and resident memory T cells following skin immunization. *Nat. Med.* 21:647–653. http://dx.doi.org/10.1038/nm.3860

Galea, I., I. Bechmann, and V.H. Perry. 2007. What is immune privilege (not)? *Trends Immunol.* 28:12–18. http://dx.doi.org/10.1016/j.it.2006.11.004

Gebhardt, T., L.M. Wakim, L. Eidsmo, P.C. Reading, W.R. Heath, and F.R. Carbone. 2009. Memory T cells in nonlymphoid tissue that provide enhanced local immunity during infection with herpes simplex virus. *Nat. Immunol.* 10:524–530. http://dx.doi.org/10.1038/ni.1718

Gilden, D.H., R. Mahalingam, R.J. Cohrs, and K.L. Tyler. 2007. Herpesvirus infections of the nervous system. *Nat. Clin. Pract. Neurol.* 3:82–94. http://dx.doi.org/10.1038/ncpneuro0401

Graef, P., V.R. Buchholz, C. Stemberger, M. Flossdorf, L. Henkel, M. Schiemann, I. Drexler, T. Höfer, S.R. Riddell, and D.H. Busch. 2014. Serial transfer of single-cell-derived immunocompetence reveals stemness of CD8(+) central memory T cells. *Immunity.* 41:116–126. http://dx.doi.org/10.1016/j.immuni.2014.05.018

Griffin, D.E. 2003. Immune responses to RNA-virus infections of the CNS. *Nat. Rev. Immunol.* 3:493–502. http://dx.doi.org/10.1038/nri1105

Hand, T.W., W. Cui, Y.W. Jung, E. Sefik, N.S. Joshi, A. Chandele, Y. Liu, and S.M. Kaech. 2010. Differential effects of STAT5 and PI3K/AKT signaling on effector and memory CD8 T-cell survival. *Proc. Natl. Acad. Sci. USA.* 107:16601–16606. http://dx.doi.org/10.1073/pnas.1003457107

Herz, J., K.R. Johnson, and D.B. McGavern. 2015. Therapeutic antiviral T cells noncytopathically clear persistently infected microglia after conversion into antigen-presenting cells. *J. Exp. Med.* 212:1153–1169. http://dx.doi.org/10.1084/jem.20142047

Hogquist, K.A., S.C. Jameson, W.R. Heath, J.L. Howard, M.J. Bevan, and F.R. Carbone. 1994. T cell receptor antagonist peptides induce positive selection. *Cell.* 76:17–27. http://dx.doi.org/10.1016/0092-8674(94)90169-4

Iwasaki, A., and R. Medzhitov. 2015. Control of adaptive immunity by the innate immune system. *Nat. Immunol.* 16:343–353. http://dx.doi.org/10.1038/ni.3123

Jiang, X., R.A. Clark, L. Liu, A.J. Wagers, R.C. Fuhlbrigge, and T.S. Kupper. 2012. Skin infection generates non-migratory memory CD8$^+$ T(RM) cells providing global skin immunity. *Nature.* 483:227–231. http://dx.doi.org/10.1038/nature10851

Johnson, S., A. Bergthaler, F. Graw, L. Flatz, W.V. Bonilla, C.A. Siegrist, P.H. Lambert, R.R. Regoes, and D.D. Pinschewer. 2015. Protective efficacy of individual CD8$^+$ T cell specificities in chronic viral infection. *J. Immunol.* 194:1755–1762. http://dx.doi.org/10.4049/jimmunol.1401771

Kägi, D., B. Ledermann, K. Bürki, P. Seiler, B. Odermatt, K.J. Olsen, E.R. Podack, R.M. Zinkernagel, and H. Hengartner. 1994. Cytotoxicity mediated by T cells and natural killer cells is greatly impaired in perforin-deficient mice. *Nature.* 369:31–37. http://dx.doi.org/10.1038/369031a0

Kohlmeier, J.E., T. Cookenham, A.D. Roberts, S.C. Miller, and D.L. Woodland. 2010. Type I interferons regulate cytolytic activity of memory CD8$^+$ T cells in the lung airways during respiratory virus challenge. *Immunity.* 33:96–105. http://dx.doi.org/10.1016/j.immuni.2010.06.016

Laidlaw, B.J., N. Zhang, H.D. Marshall, M.M. Staron, T. Guan, Y. Hu, L.S. Cauley, J. Craft, and S.M. Kaech. 2014. CD4$^+$ T cell help guides formation of CD103$^+$ lung-resident memory CD8$^+$ T cells during influenza viral infection. *Immunity.* 41:633–645. http://dx.doi.org/10.1016/j.immuni.2014.09.007

Liu, L., Q. Zhong, T. Tian, K. Dubin, S.K. Athale, and T.S. Kupper. 2010. Epidermal injury and infection during poxvirus immunization is crucial for the generation of highly protective T cell-mediated immunity. *Nat. Med.* 16:224–227. http://dx.doi.org/10.1038/nm.2078

Mackay, L.K., A. Rahimpour, J.Z. Ma, N. Collins, A.T. Stock, M.L. Hafon, J. Vega-Ramos, P. Lauzurica, S.N. Mueller, T. Stefanovic, et al. 2013. The developmental pathway for CD103(+)CD8$^+$ tissue-resident memory T cells of skin. *Nat. Immunol.* 14:1294–1301. http://dx.doi.org/10.1038/ni.2744

Mackay, L.K., A. Braun, B.L. Macleod, N. Collins, C. Tebartz, S. Bedoui, F.R. Carbone, and T. Gebhardt. 2015a. Cutting edge: CD69 interference with sphingosine-1-phosphate receptor function regulates peripheral T cell retention. *J. Immunol.* 194:2059–2063. http://dx.doi.org/10.4049/jimmunol.1402256

Mackay, L.K., E. Wynne-Jones, D. Freestone, D.G. Pellicci, L.A. Mielke, D.M. Newman, A. Braun, F. Masson, A. Kallies, G.T. Belz, and F.R. Carbone. 2015b. T-box Transcription Factors Combine with the Cytokines TGF-β and IL-15 to Control Tissue-Resident Memory T Cell Fate. *Immunity.* 43:1101–1111. http://dx.doi.org/10.1016/j.immuni.2015.11.008

McCausland, M.M., and S. Crotty. 2008. Quantitative PCR technique for detecting lymphocytic choriomeningitis virus in vivo. *J. Virol. Methods.* 147:167–176. http://dx.doi.org/10.1016/j.jviromet.2007.08.025

McGavern, D.B., and S.S. Kang. 2011. Illuminating viral infections in the nervous system. *Nat. Rev. Immunol.* 11:318–329. http://dx.doi.org/10.1038/nri2971

McNab, F., K. Mayer-Barber, A. Sher, A. Wack, and A. O'Garra. 2015. Type I interferons in infectious disease. *Nat. Rev. Immunol.* 15:87–103. http://dx.doi.org/10.1038/nri3787

Mueller, S.N., T. Gebhardt, F.R. Carbone, and W.R. Heath. 2013. Memory T cell subsets, migration patterns, and tissue residence. *Annu. Rev. Immunol.* 31:137–161. http://dx.doi.org/10.1146/annurev-immunol-032712-095954

Neumann, H., A. Cavalié, D.E. Jenne, and H. Wekerle. 1995. Induction of MHC class I genes in neurons. *Science.* 269:549–552. http://dx.doi.org/10.1126/science.7624779

Oehen, S., H. Hengartner, and R.M. Zinkernagel. 1991. Vaccination for disease. *Science.* 251:195–198. http://dx.doi.org/10.1126/science.1824801

Park, C.O., and T.S. Kupper. 2015. The emerging role of resident memory T cells in protective immunity and inflammatory disease. *Nat. Med.* 21:688–697. http://dx.doi.org/10.1038/nm.3883

Pinschewer, D.D., M. Perez, A.B. Sanchez, and J.C. de la Torre. 2003. Recombinant lymphocytic choriomeningitis virus expressing vesicular stomatitis virus glycoprotein. *Proc. Natl. Acad. Sci. USA.* 100:7895–7900. http://dx.doi.org/10.1073/pnas.1332709100

Pinschewer, D.D., M. Schedensack, A. Bergthaler, E. Horvath, W. Brück, M. Löhning, and D. Merkler. 2010. T cells can mediate viral clearance from ependyma but not from brain parenchyma in a major histocompatibility class I- and perforin-independent manner. *Brain.* 133:1054–1066. http://dx.doi.org/10.1093/brain/awq028

Pircher, H., K. Bürki, R. Lang, H. Hengartner, and R.M. Zinkernagel. 1989. Tolerance induction in double specific T-cell receptor transgenic mice varies with antigen. *Nature.* 342:559–561. http://dx.doi.org/10.1038/342559a0

Raué, H.P., C. Beadling, J. Haun, and M.K. Slifka. 2013. Cytokine-mediated programmed proliferation of virus-specific CD8(+) memory T cells. *Immunity.* 38:131–139. http://dx.doi.org/10.1016/j.immuni.2012.09.019

Rothhammer, V., A. Muschaweckh, G. Gasteiger, F. Petermann, S. Heink, D.H. Busch, M. Heikenwälder, B. Hemmer, I. Drexler, and T. Korn. 2014. α4-integrins control viral meningoencephalitis through differential recruitment of T helper cell subsets. *Acta Neuropathol. Commun.* 2:27. http://dx.doi.org/10.1186/2051-5960-2-27

Sallusto, F., D. Lenig, R. Förster, M. Lipp, and A. Lanzavecchia. 1999. Two subsets of memory T lymphocytes with distinct homing potentials and effector functions. *Nature.* 401:708–712. http://dx.doi.org/10.1038/44385

Schenkel, J.M., and D. Masopust. 2014a. Identification of a resident T-cell memory core transcriptional signature. *Immunol. Cell Biol.* 92:8–9. http://dx.doi.org/10.1038/icb.2013.67

Schenkel, J.M., and D. Masopust. 2014b. Tissue-resident memory T cells. *Immunity.* 41:886–897. http://dx.doi.org/10.1016/j.immuni.2014.12.007

Schenkel, J.M., K.A. Fraser, V. Vezys, and D. Masopust. 2013. Sensing and alarm function of resident memory $CD8^+$ T cells. *Nat. Immunol.* 14:509–513. http://dx.doi.org/10.1038/ni.2568

Schenkel, J.M., K.A. Fraser, L.K. Beura, K.E. Pauken, V. Vezys, and D. Masopust. 2014a. T cell memory. Resident memory CD8 T cells trigger protective innate and adaptive immune responses. *Science.* 346:98–101. http://dx.doi.org/10.1126/science.1254536

Schenkel, J.M., K.A. Fraser, and D. Masopust. 2014b. Cutting edge: resident memory CD8 T cells occupy frontline niches in secondary lymphoid organs. *J. Immunol.* 192:2961–2964. http://dx.doi.org/10.4049/jimmunol.1400003

Sheridan, B.S., Q.M. Pham, Y.T. Lee, L.S. Cauley, L. Puddington, and L. Lefrançois. 2014. Oral infection drives a distinct population of intestinal resident memory CD8(+) T cells with enhanced protective function. *Immunity.* 40:747–757. http://dx.doi.org/10.1016/j.immuni.2014.03.007

Shin, H., and A. Iwasaki. 2012. A vaccine strategy that protects against genital herpes by establishing local memory T cells. *Nature.* 491:463–467. http://dx.doi.org/10.1038/nature11522

Skon, C.N., J.Y. Lee, K.G. Anderson, D. Masopust, K.A. Hogquist, and S.C. Jameson. 2013. Transcriptional downregulation of S1pr1 is required for the establishment of resident memory $CD8^+$ T cells. *Nat. Immunol.* 14:1285–1293. http://dx.doi.org/10.1038/ni.2745

Soudja, S.M., A.L. Ruiz, J.C. Marie, and G. Lauvau. 2012. Inflammatory monocytes activate memory CD8(+) T and innate NK lymphocytes independent of cognate antigen during microbial pathogen invasion. *Immunity.* 37:549–562. http://dx.doi.org/10.1016/j.immuni.2012.05.029

Staib, C., I. Drexler, and G. Sutter. 2004. Construction and isolation of recombinant MVA. *Methods Mol. Biol.* 269:77–100.

Steinbach, K., M. Piedavent, S. Bauer, J.T. Neumann, and M.A. Friese. 2013. Neutrophils amplify autoimmune central nervous system infiltrates by maturing local APCs. *J. Immunol.* 191:4531–4539. http://dx.doi.org/10.4049/jimmunol.1202613

Steinert, E.M., J.M. Schenkel, K.A. Fraser, L.K. Beura, L.S. Manlove, B.Z. Igyártó, P.J. Southern, and D. Masopust. 2015. Quantifying Memory CD8 T Cells Reveals Regionalization of Immunosurveillance. *Cell.* 161:737–749. http://dx.doi.org/10.1016/j.cell.2015.03.031

Wakim, L.M., A. Woodward-Davis, and M.J. Bevan. 2010. Memory T cells persisting within the brain after local infection show functional adaptations to their tissue of residence. *Proc. Natl. Acad. Sci. USA.* 107:17872–17879. http://dx.doi.org/10.1073/pnas.1010201107

Wakim, L.M., A. Woodward-Davis, R. Liu, Y. Hu, J. Villadangos, G. Smyth, and M.J. Bevan. 2012. The molecular signature of tissue resident memory CD8 T cells isolated from the brain. *J. Immunol.* 189:3462–3471. http://dx.doi.org/10.4049/jimmunol.1201305

Willinger, T., T. Freeman, H. Hasegawa, A.J. McMichael, and M.F. Callan. 2005. Molecular signatures distinguish human central memory from effector memory CD8 T cell subsets. *J. Immunol.* 175:5895–5903. http://dx.doi.org/10.4049/jimmunol.175.9.5895